Search for associated production of dark matter with a Higgs boson decaying to $\mathrm{b\bar{b}}$ or $\gamma\gamma$ at $\sqrt{s} = 13$ TeV

The CMS collaboration

E-mail: cms-publication-committee-chair@cern.ch

Abstract: A search for dark matter is performed looking for events with large missing transverse momentum and a Higgs boson decaying either to a pair of bottom quarks or to a pair of photons. The data from proton-proton collisions at a center-of-mass energy of 13 TeV, collected in 2015 with the CMS detector at the LHC, correspond to an integrated luminosity of 2.3 fb^{-1}. Results are interpreted in the context of a Z'-two-Higgs-doublet model, where the gauge symmetry of the standard model is extended by a U(1)$_{Z'}$ group, with a new massive Z' gauge boson, and the Higgs sector is extended with four additional Higgs bosons. In this model, a high-mass resonance Z' decays into a pseudoscalar boson A and a light SM-like scalar Higgs boson, and the A decays to a pair of dark matter particles. No significant excesses are observed over the background prediction. Combining results from the two decay channels yields exclusion limits in the signal cross section in the $m_{Z'}$-m_A phase space. For example, the observed data exclude the Z' mass range from 600 to 1860 GeV, for Z' coupling strength $g_{Z'} = 0.8$, the coupling of A with dark matter particles $g_\chi = 1$, the ratio of the vacuum expectation values $\tan\beta = 1$, and $m_A = 300$ GeV. The results of this analysis are valid for any dark matter particle mass below 100 GeV.

Contents

1 Introduction

Astrophysical observations have provided strong evidence for the existence of dark matter (DM) in the universe [1]. However, its underlying nature remains unknown and cannot be accommodated within the standard model (SM). The recent discovery of a Higgs boson with mass of about 125 GeV by the ATLAS and CMS experiments [2–4] provides an additional handle to probe the dark sector beyond the SM. As explained below, in the analyses presented here, it is assumed that there are five physical Higgs bosons, and that the new state corresponds to the light neutral CP-even state h. If DM has origin in particle physics, and if other than gravitational interactions exist between DM and SM particles, DM particles (χ) could be produced at the CERN LHC. One way to observe DM particles would be through their recoil against a SM particle X (X = g, q, γ, Z, W, or h) that is produced in association with the DM. This associated production of DM and SM particles is often referred to as mono-X production. The SM particle X can be emitted directly from a quark or gluon as initial-state radiation, or through a new interaction between DM and SM particles, or as final-state radiation. The Higgs boson radiation from an initial-state quark or gluon is suppressed through Yukawa or loop processes, respectively. A scenario in
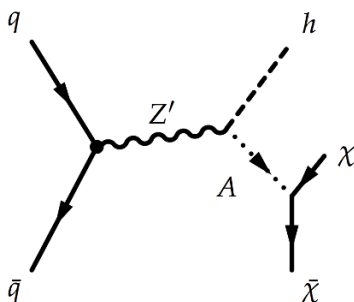
Figure 1. Leading order Feynman diagram of the Z'-2HDM "simplified model". A pseudoscalar boson A decaying into invisible dark matter is produced from the decay of an on-shell Z' resonance. This gives rise to a Higgs boson and missing transverse momentum.

which the Higgs boson is part of the interaction producing the DM particles gives mono-h searches a uniquely enhanced sensitivity to the structure of couplings between the SM particles and the dark matter [5–7]. At the LHC, searches for DM in the mono-h channel have been performed by the ATLAS Collaboration using data corresponding to integrated luminosities of $20\,\mathrm{fb}^{-1}$ at $\sqrt{s} = 8\,\mathrm{TeV}$ and $3.2\,\mathrm{fb}^{-1}$ at $\sqrt{s} = 13\,\mathrm{TeV}$, through the decay channels $h \to b\bar{b}$ [8, 9] and $h \to \gamma\gamma$ [10].

In this paper, a search for DM is presented in the mono-h channel in which the Higgs boson decays to either a pair of bottom quarks ($b\bar{b}$) or photons ($\gamma\gamma$). The results have been interpreted using a benchmark "simplified model" recommended in the ATLAS-CMS Dark Matter Forum, which is described in ref. [11]: a Z'-two-Higgs-doublet-model (Z'-2HDM) [7], where a heavy Z' vector boson is produced resonantly and decays into a SM-like Higgs boson h and an intermediate heavy pseudoscalar particle A, which in turn decays into a pair of DM particles, as shown in figure 1.

In the Z'-2HDM model, the gauge symmetry of the SM is extended by a $U(1)_{Z'}$ group, with a new massive Z' gauge boson. A Type-2 2HDM [12, 13] is used to formulate the extended Higgs sector. A doublet Φ_u couples only to up-type quarks, and a doublet Φ_d couples to down-type quarks and leptons. Only Φ_u and right-handed up-type quarks u_R have an associated charge under the $U(1)_{Z'}$ group, while Φ_d and all other SM fermions are neutral. After electroweak symmetry breaking, the Higgs doublets attain vacuum expectation values v_u and v_d, resulting in five physical Higgs bosons: a light neutral CP-even scalar h, assumed to be the observed 125 GeV Higgs boson, a heavy neutral CP-even scalar H, a neutral CP-odd scalar A, and two charged scalars $H^\pm$. The analysis in this paper is performed in the context of the so-called alignment limit where the h has SM-like couplings to fermions and gauge bosons, and the ratio of the vacuum expectation values $\tan\beta = v_u/v_d > 0.3$, as implied from the perturbativity limit of the Yukawa coupling [7, 14] of the top quark, the h-H mixing angle α is related to β by $\alpha = \beta - \pi/2$.

The benchmark model is parametrized through six quantities: (i) the pseudoscalar mass m_A, (ii) the DM mass m_χ, (iii) the Z' mass $m_{Z'}$, (iv) $\tan\beta$, (v) the Z' coupling strength $g_{Z'}$, and (vi) the coupling constant between the A and DM particles g_χ.

Only the masses m_A and $m_{Z'}$ affect the kinematic distributions of the objects in the final states studied in this analysis. In fact, when A is on-shell, i.e. $m_A > 2m_\chi$, the distri-

butions have little dependence on m_χ. The remaining parameters modify the production cross section of Z', branching fraction, and decay widths of the Z' and the A, resulting in only small changes to the final-state kinematic distributions.

This paper considers a Z' resonance with mass between 600 and 2500 GeV and an A with mass between 300 and 800 GeV, while the mass of DM particles m_χ is less than or equal to 100 GeV. The parameters $\tan\beta$ and g_χ are fixed at unity and two different assumptions on $g_{Z'}$ are evaluated as described in more detail later. Values of m_A below 300 GeV are excluded by constraints on flavor changing neutral currents from measurements of b $\rightarrow$ sγ [13], and are not considered here.

The branching fraction for decays of A to DM particles, $\mathcal{B}(\mathrm{A} \rightarrow \chi\overline{\chi})$, decreases as m_χ increases; for the range of m_A considered in this paper, the relative decrease of $\mathcal{B}(\mathrm{A} \rightarrow \chi\overline{\chi})$ is less than 7% as m_χ increases from 0 to 100 GeV. Therefore, although signals with $m_\chi = 100$ GeV are considered in this search, the results are valid for any value of dark matter particle mass below 100 GeV.

The results presented here consider only A decays to DM particles and the final signal cross section $\sigma(\mathrm{Z'} \rightarrow \mathrm{Ah} \rightarrow \chi\overline{\chi}\mathrm{h})$ includes the value of $\mathcal{B}(\mathrm{A} \rightarrow \chi\overline{\chi})$. With the assumed dark matter particle mass, the value of $\mathcal{B}(\mathrm{A} \rightarrow \chi\overline{\chi})$ is $\approx 100\%$ for $m_A = 300$ GeV. The branching fraction starts to decrease for m_A greater than twice the mass of the top quark as the decay A $\rightarrow$ t$\overline{\mathrm{t}}$ becomes kinematically accessible. For example, if $m_A = 400\,(800)$ GeV, $\mathcal{B}(\mathrm{A} \rightarrow \chi\overline{\chi})$ reduces to 54 (42)%.

The quantity $\vec{p}_\mathrm{T}^{\,\mathrm{miss}}$, calculated as the negative vectorial sum of the transverse momentum (p_T) of all objects identified in an event, represents the total momentum carried by the DM particles. The magnitude of this vector is referred to as $p_\mathrm{T}^\mathrm{miss}$. For a given value of $m_{Z'}$, the p_T of the A decreases as m_A increases. Therefore, the $p_\mathrm{T}^\mathrm{miss}$ spectrum softens with increasing m_A. A comparison of the $p_\mathrm{T}^\mathrm{miss}$ distributions for three values of m_A is shown in figure 2.

The signal cross section is calculated for two assumptions on $g_{Z'}$: (i) a fixed value of $g_{Z'}$ = 0.8, as considered in ref. [9] and recommended in ref. [11], and (ii) using the maximum value from electroweak global fits and constraints from dijet searches [7]:

$$g_{Z'} = 0.03 \, \frac{g_\mathrm{W}}{\cos\theta_\mathrm{W} \sin^2\beta} \, \frac{\sqrt{m_{Z'}^2 - m_Z^2}}{m_Z}, \tag{1.1}$$

yielding $g_{Z'} = 0.485$ for $m_{Z'} = 1$ TeV, and $g_{Z'} = 0.974$ for $m_{Z'} = 2$ TeV. It can be seen from eq. (1.1) that $g_{Z'} = 0.8$ is the maximum allowed value of $g_{Z'}$ for $\tan\beta = 1$ and $m_{Z'} = 1.7$ TeV (the best reach of LHC as estimated by ref. [7]). Note that this analysis does not consider the contribution of another decay that gives a similar mono-h signature: Z' $\rightarrow$ Zh where Z $\rightarrow \nu\overline{\nu}$. The ratio of branching fractions, $\mathcal{B}(\mathrm{Z'} \rightarrow \mathrm{Zh}, \mathrm{Z} \rightarrow \nu\overline{\nu})/\mathcal{B}(\mathrm{Z'} \rightarrow \mathrm{Ah}, \mathrm{A} \rightarrow \chi\overline{\chi})$, is a function of $\tan\beta$ and $m_{Z'}$ and does not depend on $g_{Z'}$ since the value of $g_{Z'}$ cancels in the ratio.

The h $\rightarrow$ b$\overline{\mathrm{b}}$ decay mode has the largest branching fraction ($\approx$58%) of all, but suffers from relatively poor mass resolution of about 10%, and while the h $\rightarrow \gamma\gamma$ branching fraction is small ($\approx$0.2%), the channel benefits from the high precision in reconstructed diphoton mass, with a resolution of about 1–2%.
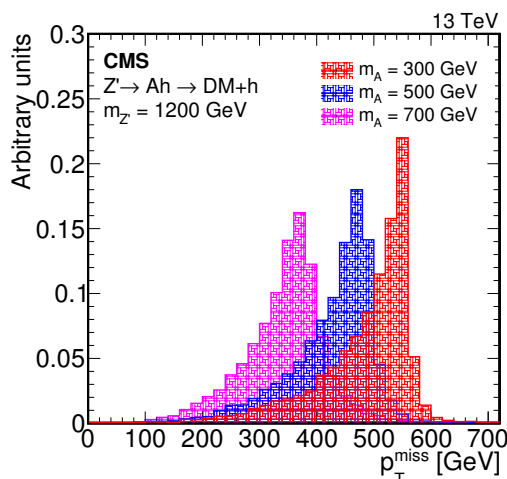
Figure 2. Distribution of p_T^{miss} at generator level for $Z' \to A\,h \to DM+h$ with $m_A = 300, 500,$ and $700\,GeV$ with $m_{Z'} = 1200\,GeV$. All other parameters of the model are fixed, as mentioned in the text.

In the $h \to b\bar{b}$ channel, the fact that the p_T of the h should increase with $m_{Z'}$ and decrease with m_A is exploited. The minimum separation in the pseudorapidity and azimuth (η, ϕ) plane between the decay products of h scales as m_h/p_T^h, where p_T^h is the transverse momentum of the h boson. The allowed mass ranges of $m_{Z'}$ and m_A imply a very wide range of values for p_T^h and consequently a wide range in the separation of the decay products. Analysis in this channel is therefore divided into two regimes: (i) a resolved regime where the h decays to two distinct reconstructed b jets, and (ii) a Lorentz-boosted regime where the h is reconstructed as a single fat jet. For each mass point, the analysis with best sensitivity for the expected limit is used as the final result. The signal extraction is performed through a simultaneous fit to the signal- and background-enriched control regions.

The search in the $h \to \gamma\gamma$ channel is performed by seeking an excess of events over the SM prediction in the diphoton mass spectrum, after requiring a large p_T^{miss}. Control samples in data are used to estimate the reducible background, which mainly consists of diphoton SM production. A counting approach is used to estimate the potential signal.

The paper is organized as follows. After a brief introduction to the CMS detector in section 2, the data and simulated events used for the analysis are described in section 3. The event reconstruction is detailed in section 4. Section 5 describes the analysis strategy for both Higgs boson decay channels. The description of the most relevant systematic uncertainties affecting the analysis is found in section 6. Finally, the results of the search are reported in section 7, and the summary is presented in section 8.

2   The CMS detector

The central feature of the CMS detector is a superconducting solenoid, of 6 m internal diameter, providing an axial magnetic field of 3.8 T along the beam direction. Within the

solenoid volume are a silicon pixel and strip tracker, a lead tungstate crystal electromagnetic calorimeter (ECAL), and a brass and scintillator hadron calorimeter (HCAL). Charged particle trajectories are measured by the silicon pixel and strip tracker system, covering $0 \leq \phi \leq 2\pi$ in azimuth and $|\eta| < 2.5$. The electromagnetic calorimeter, which surrounds the tracker volume, consists of 75,848 lead tungstate crystals that provide coverage in pseudorapidity $|\eta| < 1.48$ in the barrel region (EB) and $1.48 < |\eta| < 3.0$ in two endcap regions (EE). The EB modules are arranged in projective towers. A preshower detector consisting of two planes of silicon sensors interleaved with a total of three radiation lengths of lead is located in front of the EE. In the region $|\eta| < 1.74$, the HCAL cells have widths of 0.087 in pseudorapidity and azimuth. In the (η, ϕ) plane and for $|\eta| < 1.48$, the HCAL cells map on to 5×5 ECAL crystal arrays to form calorimeter towers projecting radially outwards from the nominal interaction point. For $|\eta| > 1.74$, the coverage of the towers increases progressively to a maximum of 0.174 in $\Delta\eta$ and $\Delta\phi$. Extensive forward calorimetry complements the coverage provided by the barrel and endcap calorimeters. Muons are measured in gas-ionization detectors embedded in the steel return yoke. A more detailed description of the CMS detector can be found in ref. [15].

3   Data and simulated samples

The analysis is performed with pp collision data at $\sqrt{s} = 13\,\text{TeV}$ collected by the CMS experiment at the LHC during 2015, corresponding to an integrated luminosity of $2.3\,\text{fb}^{-1}$.

The MadGraph5_aMC@NLO v2.3.0 [16] generator is used to generate the mono-h signal at leading order (LO) as predicted by the Z′-2HDM model described in section 1. In the MadGraph5_aMC@NLO generation, a vector particle Z′ that decays to a SM-like Higgs boson h with mass 125 GeV is produced resonantly together with a heavy pseudoscalar particle A that decays into a pair of DM particles. The decay of the SM-like Higgs boson is handled by pythia 8.205 [17].

The associated production of a SM Higgs boson and a Z boson (Zh) is a small but irreducible background for both decay channels. The Vh (Zh and Wh) processes are simulated using powheg v2.0 [18, 19] and MadGraph5_aMC@NLO for q$\overline{\text{q}}$ and gluon-gluon fusion, respectively. In the h $\rightarrow \gamma\gamma$ channel, additional resonant but reducible backgrounds are considered. These backgrounds include the SM Higgs boson, produced through gluon fusion (ggh), through vector boson fusion (VBF), and in association with top quarks (t$\overline{\text{t}}$h). All of these resonant backgrounds are modeled at next-to-leading order (NLO) in simulation. The VBF Higgs boson samples are generated using powheg [20], while the ggh and t$\overline{\text{t}}$h samples are generated with MadGraph5_aMC@NLO.

The dominant background processes for the h $\rightarrow$ b$\overline{\text{b}}$ decay channel are events with top quarks and W/Z bosons produced in association with jets. The t$\overline{\text{t}}$ events, produced via the strong interaction, and electroweak production of single top quarks in the t- and tW-channels are generated at NLO with powheg [21–25]. The s-channel process of single top quark production is generated with MadGraph5_aMC@NLO. Differential measurements of top quark pair production show that the measured p_{T} spectrum of top quarks is softer than the one produced in simulation. Scale factors to correct for this effect are

derived from previous CMS measurements [26, 27]. The sum of top quark pair events and single top quark events is referred to as "Top quark background" in the rest of the paper. The W and Z boson production in association with jets is simulated at LO with MadGraph5_amc@nlo. Up to four additional partons in the matrix element calculations are included. The MLM matching scheme [28] is used as an interface to the parton shower generated with pythia. The cross sections for W+jets and Z+jets processes are normalized to the next-to-next-to-leading order cross section, computed using fewz v3.1 [29]. Moreover, to improve the description of the distribution of high p_T W+jets and Z+jets processes, events are reweighted using the generated p_T of the vector boson to account for NLO quantum chromodynamics (QCD) and electroweak (EW) contributions [30–32]. The small background from diboson (WW, WZ, and ZZ) processes, labeled as VV in the rest of the paper, is simulated with pythia.

For the h → γγ decay channel, several nonresonant background sources can mimic the signal when an event has mismeasured p_T^{miss} and two photons with an invariant mass close to the mass of the SM-like Higgs boson. These sources include contributions from dijet and multijet events, EW processes such as t, $t\bar{t}$, Z, ZZ, or W bosons produced in association with one or two photons, γγ, γ+jet, and Drell-Yan (DY) production in association with jets, where the Z boson decays to pairs of electrons and neutrinos. These backgrounds are generated with MadGraph5_amc@nlo, with the exception of the ZZ sample, which is generated with powheg [33]. These nonresonant background samples are not used for the background estimation, but are used to optimize the selection.

All simulated samples use the NNPDF 3.0 PDF sets [34]. The parton showering and hadronization are performed with pythia using the CUETP8M1 tune [35, 36]. For the h → b$\bar{b}$ decay channel, to perform systematic studies in the boosted regime, an additional signal sample is generated with MadGraph5_amc@nlo, parton-showered and hadronized by herwig++ v2.7.1 [37] using the UE-EE-5C tune [38, 39]. The samples are processed through a Geant4-based [40] simulation of the CMS detector. All samples include the simulation of "pileup" arising from additional inelastic proton-proton interactions in the same or neighboring bunch crossings. An average of approximately ten pileup interactions per bunch crossing is included in the simulation with a separation between bunches of 25 ns. The simulated pileup distribution is reweighted to match the corresponding observed distribution in the analyzed data.

4 Event reconstruction

A global event reconstruction is performed using the particle-flow (PF) [41–43] algorithm, which optimally combines the information from all the subdetectors and produces a list of stable particles, namely muons, electrons, photons, charged and neutral hadrons.

The reconstructed interaction vertex with the largest value of $\sum_i p_{Ti}^2$, where p_{Ti} is the transverse momentum of the ith track associated with the vertex, is selected as the primary event vertex. This vertex is used as the reference vertex for all objects reconstructed using the PF algorithm. The offline selection requires all events to have at least one primary

vertex reconstructed within a 24 cm window along the z-axis around the mean interaction point, and a transverse distance from the mean interaction region less than 2 cm.

Jets are reconstructed from the PF candidates, after removing charged hadrons originating from pileup vertices, using the anti-k_T clustering algorithm [44] with distance parameters of 0.4 (AK4 jet) and 0.8 (AK8 jet), as implemented in the FASTJET package [45]. In order to improve the discrimination of signal against multijet background, the pruning algorithm described in refs. [46, 47], which is designed to remove contributions from soft radiation and pileup, is applied to AK8 jets. The pruned jet mass ($m^\mathrm{pruned}_\mathrm{corrected}$) is defined as the invariant mass associated with the four-momentum of the pruned jet, after the application of the jet energy corrections [48]. Corrections to jet momenta are further propagated to the $p^\mathrm{miss}_\mathrm{T}$ calculation [49]. In addition, tracks with $p_\mathrm{T} > 1\,\mathrm{GeV}$, $|\eta| < 2.5$, and with longitudinal impact parameter $|d_Z| < 0.1\,\mathrm{cm}$ from the primary vertex are used to reconstruct the track-based missing transverse momentum vector, $\vec{p}^{\,\mathrm{miss}}_\mathrm{T,trk}$.

The jets originating from the decay of b quarks are identified using the combined secondary vertex (CSV) algorithm [50, 51], which uses PF jets as inputs. The algorithm combines the information from the primary vertex, track impact parameters, and secondary vertices within the jet using a neural network discriminator. The loose (medium) working point (WP) used in this analysis has a b jet selection efficiency of 83% (69%), a charm jet selection efficiency of 28% (20%), and a mistag rate for light-flavor jets of $\approx$10% (1%) [50]. The AK8 jets are split into two subjets using the soft-drop algorithm [52, 53]. The CSV algorithm is tested and validated for AK4 and AK8 jets [50]. The working points for the analyses of the resolved and boosted regimes were chosen by maximizing the expected significance. The loose WP of the subjet b tagging algorithm is used for the boosted regime, whereas the medium WP of the AK4 jet b tagging algorithm is used for the resolved regime, since the background is higher in this case.

Photons are reconstructed in the CMS detector from their energy deposits in the ECAL, which come from an electromagnetic shower involving several crystals. The energy is clustered at the ECAL level by building a cluster of clusters, supercluster (SC), which is extended in the ϕ direction because of the strong magnetic field inside the detector, which deflects the electron and positron produced if the photon converts in the tracker [54]. In order to achieve the best photon energy resolution, corrections are applied to remove channel-to-channel response variations and to recover energy losses due to incomplete containment of the shower or conversions, as detailed in ref. [55]. Additional residual corrections are made to the measured energy scale of the photons in data ($\leq$1%) and to the energy resolution in simulation ($\leq$2%) based on a detailed study of the mass distribution of $\mathrm{Z} \to \mathrm{e}^+\mathrm{e}^-$ events. The uncertainties in the measurements of the photon energy scale and resolution are taken as systematic uncertainties as described in section 6. This process is outlined for the 8 TeV data set in ref. [55]. Values are adjusted for the 13 TeV data set.

Electron reconstruction requires the matching of a supercluster in the ECAL with a track in the silicon tracker. Identification criteria [56] are based on the ECAL shower shape. Muons are reconstructed by combining two complementary algorithms [57]: one in which tracks in the silicon tracker are matched to a muon track segment, and another

in which a global track fit is performed, seeded by the muon track segment. Further identification criteria are imposed on muon candidates to reduce the number of misidentified hadrons. Hadronically decaying τ leptons (τ_h) are reconstructed using the hadron-plus-strips algorithm [58], which uses the charged-hadron and neutral-electromagnetic objects to reconstruct intermediate resonances into which the τ lepton decays.

5 Event selection and background estimation

This analysis searches for excesses over the background-only prediction in events with large $p_\mathrm{T}^\mathrm{miss}$ and a system of two b-tagged jets or two photons that has a reconstructed invariant mass close to the mass of the SM-like Higgs boson h. In the h $\to$ b$\overline{\mathrm{b}}$ decay channel, the analysis relies on fitting the $p_\mathrm{T}^\mathrm{miss}$ distribution simultaneously in the signal region (SR), defined after selecting a mass window around the Higgs boson mass, and in background-enriched control regions (CRs). For the h $\to \gamma\gamma$ decay channel, a simple analysis is performed where the signal and resonant background contributions are estimated by counting the number of simulated events in the SR, while the nonresonant background is extrapolated from the data in a low-$p_\mathrm{T}^\mathrm{miss}$ region. In the following sections, the event selection and analysis strategy are described in detail for the two channels separately.

5.1 The channel h $\to$ b$\overline{\mathrm{b}}$

A search for DM produced in association with h $\to$ b$\overline{\mathrm{b}}$ is performed in a resolved regime, where events are required to have at least two AK4 jets, and in the Lorentz-boosted regime where one AK8 jet is required. In addition, $p_\mathrm{T}^\mathrm{miss}$ is required to be large because it is a key signature of the signal events and it provides strong rejection against the large reducible backgrounds described in section 3.

5.1.1 Event selection

The trigger used in the selection of signal-like events requires $p_\mathrm{T}^\mathrm{miss} > 90\,\mathrm{GeV}$ and $H_\mathrm{T}^\mathrm{miss} >$ $90\,\mathrm{GeV}$, where $H_\mathrm{T}^\mathrm{miss}$ is defined as the magnitude of the vectorial sum of the p_T of all jets in the event with $p_\mathrm{T} > 20\,\mathrm{GeV}$. An additional trigger with a $p_\mathrm{T}^\mathrm{miss} > 170\,\mathrm{GeV}$ requirement is used to achieve higher efficiency. In this way, events with either high $p_\mathrm{T}^\mathrm{miss}$ or high $H_\mathrm{T}^\mathrm{miss}$ will pass the trigger. For events passing the selection criteria that have $p_\mathrm{T}^\mathrm{miss} > 170(200)\,\mathrm{GeV}$ for the resolved (boosted) analysis, the trigger efficiency is found to be greater than 98%. The $p_\mathrm{T}^\mathrm{miss}$ threshold for the analysis of the resolved regime is set slightly lower to enhance the signal efficiency in this region of phase space, where the $p_\mathrm{T}^\mathrm{miss}$ distribution is softer.

Event filters are used to remove spurious high $p_\mathrm{T}^\mathrm{miss}$ events caused by instrumental noise in the calorimeters, or beam halo muons. It has been verified that the efficiency of these filters for accepting signal events is very close to 100%. The main part of the event selection consists of Higgs boson tagging. This selection is different for the resolved and boosted analyses. In the resolved regime, events are required to have two AK4 jets with $p_\mathrm{T} > 30\,\mathrm{GeV}$ and $|\eta| < 2.4$. These two jets are used to reconstruct the Higgs boson candidate, which is required to have $p_\mathrm{T} > 150\,\mathrm{GeV}$. Each of the two AK4 jets in the resolved regime is required to pass the b tagging selection, whereas in the boosted regime,

the two subjets inside an AK8 jet must both pass the b tagging selection. In the boosted regime, the decay products from the Higgs boson are merged. Therefore, an AK8 jet with p_{T} greater than $200\,\mathrm{GeV}$ is used to reconstruct the Higgs boson. If more than one Higgs boson candidate is reconstructed, the ambiguity is resolved by selecting the candidate with the highest p_{T}. Backgrounds due to hadronic jets are further reduced by constraining the reconstructed Higgs boson candidate mass, m_{bb}, to be between 100 and $150\,\mathrm{GeV}$. For the resolved regime, the Higgs boson candidate mass is reconstructed using two b-tagged AK4 jets. For the boosted regime, the corrected pruned mass of the AK8 jet with two b-tagged subjets is used as the Higgs boson candidate mass.

Multijet events can act as a source of background when the energy of one of the jets is mismeasured. Therefore, the absolute difference between the azimuthal angles of the vector $\vec{p}_{\mathrm{T}}^{\,\mathrm{miss}}$ and any other AK4 jet with $p_{\mathrm{T}} > 30\,\mathrm{GeV}$ is required to be greater than 0.4 radians. Multijet background is further reduced in the resolved analysis by requiring the azimuthal angle difference between the $\vec{p}_{\mathrm{T}}^{\,\mathrm{miss}}$ and $\vec{p}_{\mathrm{T,trk}}^{\,\mathrm{miss}}$ to be less than 0.7 radians.

Events are rejected if they have any isolated electron (muon) with $p_{\mathrm{T}} > 10\,\mathrm{GeV}$ and $|\eta| < 2.5$ (2.4) or any τ_{h} candidates with $p_{\mathrm{T}} > 20\,\mathrm{GeV}$ and $|\eta| < 2.3$ [56, 58, 59]. In addition, the events must not have any additional loose AK4 b-tagged jet or more than one additional AK4 jet with $p_{\mathrm{T}} > 30\,\mathrm{GeV}$ and $|\eta| < 4.5$. These vetoes considerably reduce the background from semileptonic top decay modes and leptonic decays of W+jets.

The product of the detector acceptance and selection efficiency varies from 1 to 29%, depending on the values of $m_{\mathrm{Z'}}$ and m_{A}. The average $p_{\mathrm{T}}^{\mathrm{miss}}$ increases with $m_{\mathrm{Z'}}$ and decreases with m_{A}. The overall selection efficiency, shown in table 1, follows the same trend.

5.1.2 Analysis strategy and background estimation

Several CRs are used to correct the background normalizations with dedicated scale factors. For both resolved and boosted regimes, the selection criteria of these CRs are kept as close as possible to those of the SR, except for the inversion of the additional object vetoes (leptons, jets) and the Higgs boson mass window. This makes the CRs orthogonal to the SR.

For the resolved regime, three CRs are specified: $\mathrm{Z}(\to \nu\overline{\nu})$+jets, top quark, and W+jets. The b tagging selection in all the CRs is the same as in the SR in order to minimize the b tagging systematic uncertainties when extrapolating the background scale factors measured in the CRs to the SR. The $\mathrm{Z}(\to \nu\overline{\nu})$+jets CR is defined with the same selection as the SR, except for the inversion of the reconstructed Higgs boson mass requirement. The W+jets and top quark CRs are defined by removing the mass selection and requiring exactly one isolated electron (muon) with $p_{\mathrm{T}} > 10\,\mathrm{GeV}$ and $|\eta| < 2.5$ (2.4). Events with one additional AK4 jet are placed in the top quark CR, whereas events with no additional AK4 jets enter the W+jets CR.

For the boosted regime, the $\mathrm{Z}(\to \nu\overline{\nu})$+jets CR is defined by inverting the mass requirement for the AK8 jet. Owing to the low event count and very similar topology between the W+jets and top quark backgrounds it is difficult to construct two separate CRs for W+jets and top quark backgrounds. Hence, the single-lepton CR, a combination of mainly W+jets and top quark events, is defined using the same selection as that for the signal,
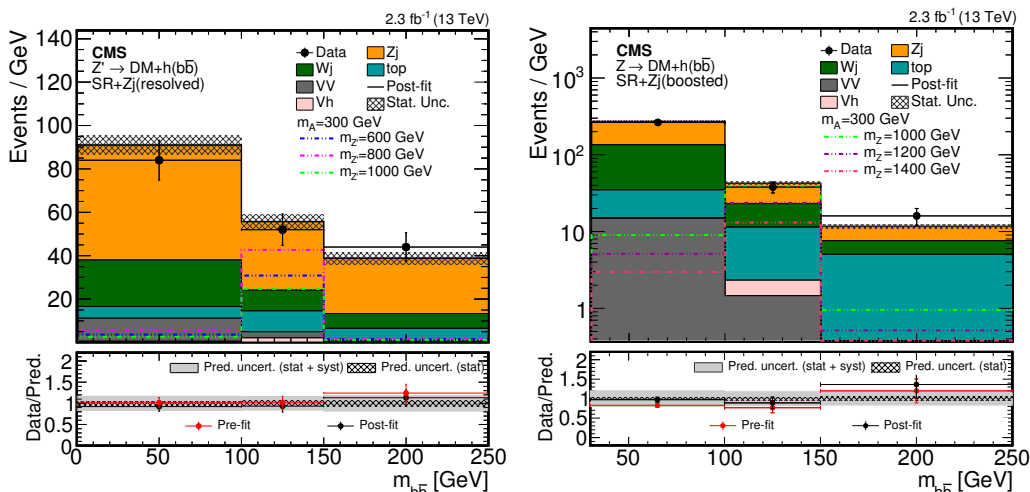
Figure 3. Post-fit distribution of the reconstructed Higgs boson candidate mass expected from SM backgrounds and observed in data for the resolved (left) and the boosted (right) regimes with three different $m_{Z'}$ signal points overlaid. Other parameters for this model are fixed to $m_\chi = 100\,\text{GeV}$ and $\tan\beta = g_\chi = 1$. The cross sections for the signal models are computed assuming $g_{Z'} = 0.8$. The bottom panels show the data-to-simulation ratios for pre-fit (red markers) and post-fit (black markers) background predictions with a hatched band corresponding to the uncertainty due to the finite size of simulated samples and a gray band that represents the systematic uncertainty in the post-fit background prediction (see section 6). The second bin represents the SR, while the events in the first and third bins are merged and represent the mass sidebands $(Z(\to\nu\bar\nu)+\text{jets})$ CR.

but requiring exactly one isolated electron (muon) with $p_T > 10\,\text{GeV}$ and $|\eta| < 2.5$ (2.4) and removing the mass requirement.

Figure 3 shows the Higgs boson candidate mass for the resolved and boosted regimes. They correspond to the simultaneous fit of the p_T^{miss} distributions in the SR and background enriched CRs to extract the signal. Data-to-simulation ratios for pre-fit and post-fit background predictions are shown in the lower panels of all figures 3–6.

Figure 4 shows the comparison of data and simulation for the main observable, p_T^{miss}, in the W+jets, top quark, and $Z(\to\nu\bar\nu)+$jets CRs for the resolved regime. The comparison between data and simulated samples for the boosted regime is shown in figure 5 for the single-lepton CR and the $Z(\to\nu\bar\nu)$ mass sideband region.

Figure 6 shows the p_T^{miss} distributions in three bins in the SR that are used for the final signal extraction. These three bins were chosen to optimize the expected limits. The selected signal and background events are compared to data and fit simultaneously in the SR and CRs in three p_T^{miss} bins, separately for the resolved and the boosted regimes.

The simultaneous fit of SR and background-enhanced CRs is performed correlating the scale factors and systematic uncertainties as described in section 6. The measured data-to-simulation post-fit scale factors are compatible with unity within the total combined statistical and systematic uncertainty. In particular, for the resolved regime, the scale factors for the backgrounds are 1.23 ± 0.17 for $Z(\to\nu\bar\nu)+$jets, 1.33 ± 0.19 for W+jets, and 1.13 ± 0.17 for the top quark contributions. For the boosted analysis, the scale factors
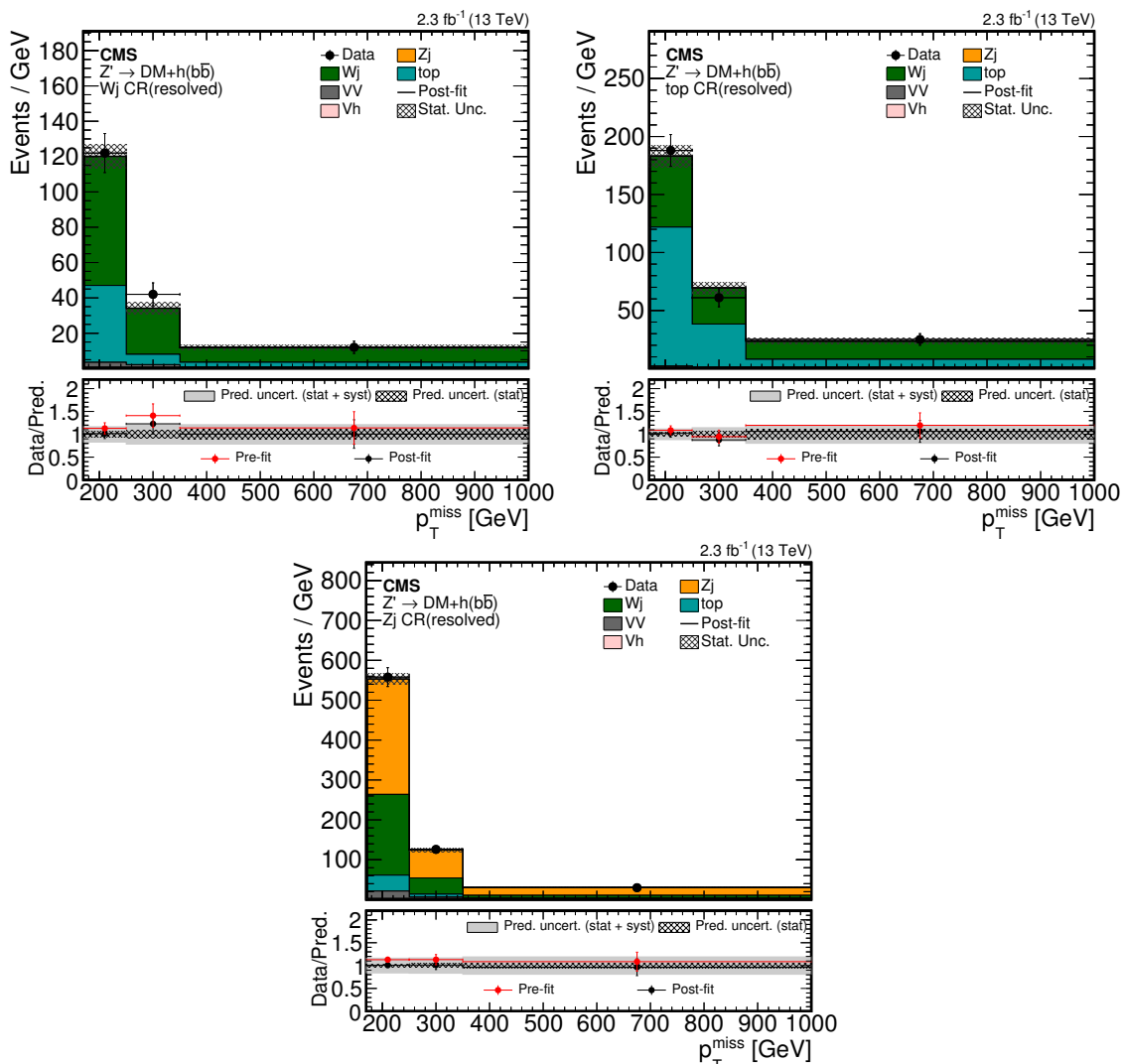
Figure 4. Post-fit distribution of p_T^{miss} expected from SM backgrounds and observed in data for the W+jets (upper left), top quark (upper right) and Z($\to \nu\bar{\nu}$)+jets (lower) CRs for the resolved regime. The bottom panels show the data-to-simulation ratios for pre-fit (red markers) and post-fit (black markers) background predictions with a hatched band corresponding to the uncertainty due to the finite size of simulated samples and a gray band that represents the systematic uncertainty in the post-fit background prediction (see section 6). The last bin includes all events with $p_T^{miss} > 350\,\text{GeV}$.

are 0.77 ± 0.15 for Z($\to \nu\bar{\nu}$)+jets and 0.95 ± 0.19 for W+jets and top quark processes. Although the background scale factors do not show a common trend between the boosted and resolved analyses, it should be noted that the b-tagging requirement, selected phase space and other parameters are different in the two cases. Thus the two simultaneous fits are essentially independent, allowing the post-fit scale factors to move in either direction from unity.
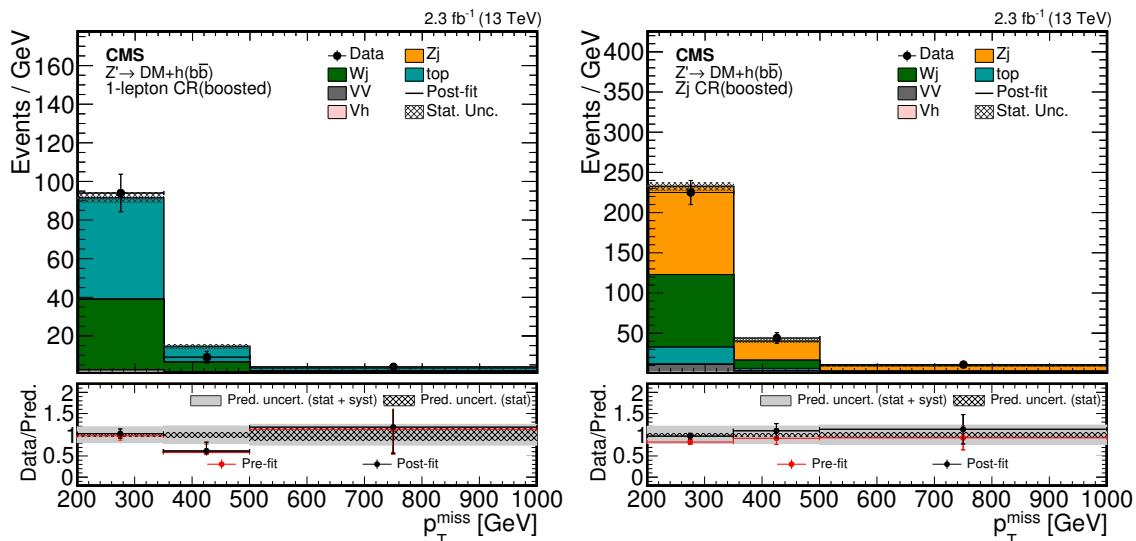
Figure 5. Post-fit distribution of p_T^{miss} expected from SM backgrounds and observed in data for the single-lepton CR and $Z(\to \nu\bar{\nu})$+jets CRs for the boosted regime. The bottom panels show the data-to-simulation ratios for pre-fit (red markers) and post-fit (black markers) background predictions with a hatched band corresponding to the uncertainty due to the finite size of simulated samples and a gray band that represents the systematic uncertainty in the post-fit background prediction (see section 6). The last bin includes all events with $p_T^{miss} > 500$ GeV.
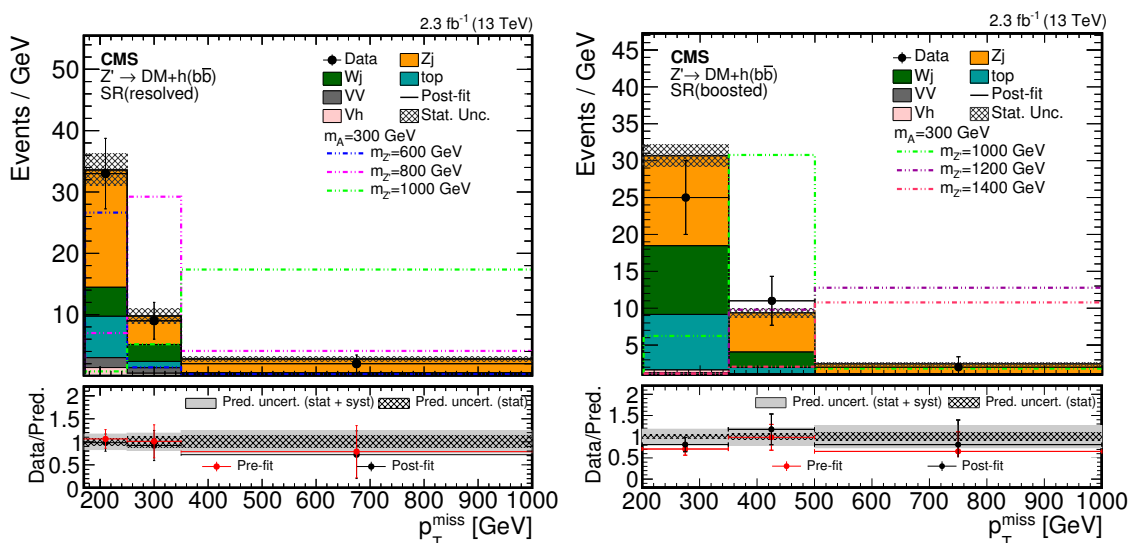
Figure 6. Post-fit distribution of p_T^{miss} expected from SM backgrounds and observed in data for the resolved (left) and the boosted (right) regimes in the signal region with three different $m_{Z'}$ signal points overlaid. Other parameters for this model are fixed to $m_\chi = 100$ GeV and $\tan\beta = g_\chi = 1$. The cross sections for the signal models are computed assuming $g_{Z'} = 0.8$. The bottom panels show the data-to-simulation ratios for pre-fit (red markers) and post-fit (black markers) background predictions with a hatched band corresponding to the uncertainty due to the finite size of simulated samples and a gray band that represents the systematic uncertainty in the post-fit background prediction (see section 6). The last bin includes all events with $p_T^{miss} > 350$ (500) GeV for the resolved (boosted) regime.

5.2 The channel h → γγ

The h → γγ search is performed using a diphoton selection. A set of requirements is applied to ensure good-quality photon candidates. Additional kinematic requirements on the objects in the final state are applied to reduce the background. The diphoton invariant mass and p_T^{miss} are used as the discriminating variables to estimate the signal.

5.2.1 Event selection

Diphoton triggers with asymmetric transverse energy thresholds ($30/18\,\text{GeV}$) are used to select events with the diphoton invariant mass above $95\,\text{GeV}$. The trigger selection uses a very loose photon identification based on the cluster shower shape and loose isolation requirements (both defined in detail in ref. [55]), and a requirement that the ratio of hadronic-to-electromagnetic energy of the photon candidates is less than 0.1.

The main source of background for photons, which arises from jets with high electromagnetic energy content, is rejected by considering the ratio of energies deposited by the photon candidate in the hadron and electromagnetic calorimeters and the spread of the energy deposition in the η direction, as described in [55]. In addition, misidentified photons are rejected using the isolation variables Iso_{Ch}, Iso_γ, and Iso_{Neu} calculated by summing the p_T of the charged hadrons, photons and neutral hadrons, respectively, in a cone of radius $\Delta R = 0.3$. In the photon identification, Iso_{Neu} and Iso_γ are corrected for the median transverse energy density (ρ) of the event to mitigate the effects of pileup [60].

The photons in the EB (i.e. the photons with $|\eta| \leq 1.44$) and photons in the EE ($1.566 \leq |\eta| \leq 2.5$) have different selection criteria, equivalent to those used in refs. [61, 62]. The working point chosen for this analysis corresponds to 90.4% (90.0%) photon ID efficiency in the EB (EE), while the misidentification rate in the EB (EE) is 16.2% (18.7%) for objects with $p_T > 20\,\text{GeV}$.

A high-quality interaction vertex, defined as the reconstructed vertex with the largest number of charged tracks, is associated to the two photons in the event. The efficiency of selecting the correct vertex for all generated mass points, defined as the fraction of signal events with well reconstructed vertices that have a z position within $1\,\text{cm}$ of the generator-level vertex, is approximately 78%.

The optimal signal selection is chosen by studying the discriminating power of variables such as the $p_T/m_{\gamma\gamma}$ of each photon, p_T^{miss}, and the p_T of the diphoton system ($p_{T\gamma\gamma}$). A selection on p_T that scales with $m_{\gamma\gamma}$ is chosen such that it does not distort the $m_{\gamma\gamma}$ spectrum shape. The $p_{T\gamma\gamma}$ variable, included because it has a better resolution than p_T^{miss}, has a distribution of values that are on average larger for signal than for background events, given that the Higgs boson is expected to be back-to-back in the transverse plane with the $\vec{p}_T^{\,miss}$.

In addition, two geometrical requirements are applied to enhance the signal over background discrimination and to veto background events with mismeasured p_T^{miss}:

- the azimuthal separation between the $\vec{p}_T^{\,miss}$ and the Higgs boson direction (reconstructed from the two photons) $|\Delta\phi(\gamma\gamma, \vec{p}_T^{\,miss})|$ must be greater than 2.1 radians.

- the minimum azimuthal angle difference between the $\vec{p}_\mathrm{T}^{\,\mathrm{miss}}$ and the jet direction in the event $min(|\Delta\phi(\mathrm{jet}, \vec{p}_\mathrm{T}^{\,\mathrm{miss}})|)$ must be greater than 0.5 radians. The jet direction is derived by considering all the jets reconstructed from the clustering of PF candidates by means of the anti-k_t algorithm [44] with a distance parameter of 0.4. Jets are considered if they have a p_T above 50 GeV in the $|\eta|$ range below 4.7 and satisfy a loose set of identification criteria designed to reject spurious detector and reconstruction effects.

The set of selection criteria that maximizes the expected significance for each Z′ mass point is studied. The optimized selection for the $m_{\mathrm{Z}'} = 600$ GeV and $m_\mathrm{A} = 300$ GeV sample maintains a large efficiency for the other signal mass points, while the backgrounds remain small. Therefore a common set of criteria is used for all signal masses with $m_{\mathrm{Z}'}$ between 600 and 2500 GeV and m_A between 300 and 800 GeV. The chosen kinematic selections include $p_{\mathrm{T}1}/m_{\gamma\gamma} > 0.5$, $p_{\mathrm{T}2}/m_{\gamma\gamma} > 0.25$, $p_{\mathrm{T}\gamma\gamma} > 90$ GeV, $p_\mathrm{T}^\mathrm{miss} > 105$ GeV. Events are vetoed if they have any muons or more than one electron present. This allows the analysis to be sensitive to events where an electron originating from conversion of the photon before reaching the ECAL is identified outside the photon supercluster. Standard lepton identification requirements are used [56, 59]. This requirement is 100% efficient for the signal and reduces significantly the EW background contributions.

The SR of this analysis is defined as the region with $120 < m_{\gamma\gamma} < 130$ GeV and $p_\mathrm{T}^\mathrm{miss}$ above 105 GeV. The distribution of $m_{\gamma\gamma}$ for the selected events before the $p_\mathrm{T}^\mathrm{miss}$ requirement is shown in figure 7 for the full mass range considered in this analysis: $105 < m_{\gamma\gamma} < 180$ GeV. Also shown is the $p_\mathrm{T}^\mathrm{miss}$ distribution of the selected events after the $m_{\gamma\gamma}$ SR selection. It can be seen that after applying the requirement that $m_{\gamma\gamma}$ has to be close to the Higgs boson mass, the SM background contribution in the high-$p_\mathrm{T}^\mathrm{miss}$ region is close to zero and the DM signal is well separated from the background distribution.

5.2.2 Background estimation

The final state with a $\gamma\gamma$ pair and large $p_\mathrm{T}^\mathrm{miss}$ has two classes of background: resonant and nonresonant. The contributions from each class are treated differently.

Resonant backgrounds arise from decays of the SM Higgs boson to two photons. They appear as an additional peak under the expected signal peak and are evaluated with the MC simulation by counting the number of expected events from all SM Higgs production modes in the SR.

The contribution of the nonresonant backgrounds ($N_\mathrm{SB}^\mathrm{bkg}$) in the sideband (SB) region, mostly multijets and EW processes with mismeasured large $p_\mathrm{T}^\mathrm{miss}$ and misidentified photons, is evaluated from the data by counting the number of events in the $m_{\gamma\gamma}$ sidebands $105 < m_{\gamma\gamma} < 120$ GeV and $130 < m_{\gamma\gamma} < 180$ GeV, with $p_\mathrm{T}^\mathrm{miss} > 105$ GeV in both cases. Then $N_\mathrm{SB}^\mathrm{bkg}$ is scaled by a transfer factor α to take into account the relative fraction between the number of events in the $m_{\gamma\gamma}$ SR and SB region. The expected number of nonresonant background events in the SR is given by:

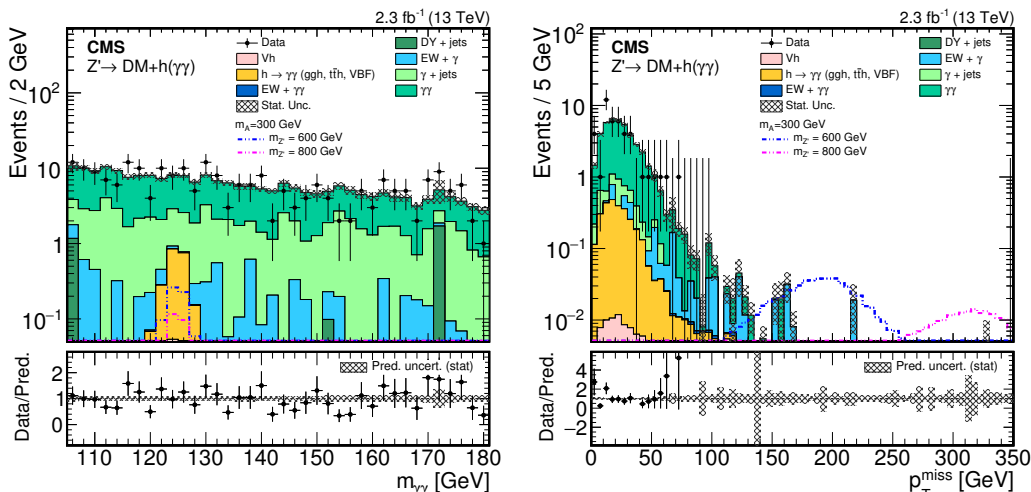$$N_\mathrm{SR}^\mathrm{bkg} = \alpha N_\mathrm{SB}^\mathrm{bkg}. \tag{5.1}$$

Figure 7. Expected and observed distribution of $m_{\gamma\gamma}$ (left) in events passing all selection criteria except the $m_{\gamma\gamma}$ and p_T^{miss} requirement. Expected and observed distribution of p_T^{miss} (right) for events passing all selection criteria including $120\,\text{GeV} < m_{\gamma\gamma} < 130\,\text{GeV}$ except p_T^{miss} requirement. Two different $m_{Z'}$ signal points are overlaid. Other parameters for this model are fixed to $m_\chi = 100\,\text{GeV}$ and $\tan\beta = g_\chi = 1$. The cross sections for the signal models are computed assuming $g_{Z'} = 0.8$. For both plots, the total simulated background is normalized to the total number of events in data. The bottom panels show the data-to-simulation ratios for background predictions with a hatched band corresponding to the uncertainty due to the finite size of simulated samples.

The derivation of α relies on the knowledge of the background shape $f_{bkg}(m_{\gamma\gamma})$ as follows:

$$\alpha = \frac{\int_{SR} f_{bkg}(m_{\gamma\gamma})\mathrm{d}m_{\gamma\gamma}}{\int_{SB} f_{bkg}(m_{\gamma\gamma})\mathrm{d}m_{\gamma\gamma}}, \tag{5.2}$$

and is evaluated by performing a fit to the $m_{\gamma\gamma}$ distribution in a CR of the data. In this analysis, the low-p_T^{miss} CR, with $p_T^{miss} < 105\,\text{GeV}$, is used. The fit to data in the low-p_T^{miss} region used to calculate α is shown in figure 8. In this case the negligible contribution of the resonant SM Higgs boson processes is not considered. The data are fit with a background-only model using an analytic power law function:

$$f(x) = ax^{-b} \tag{5.3}$$

where the parameter a, the normalization, and b are free parameters, defined as positive. The fit is performed with an unbinned maximum likelihood technique. The function defined in eq. (5.3) was chosen after examining several models and performing a bias study using nonresonant background MC to evaluate any possible background mismodeling, following the procedure described in ref. [63]. It has been verified that the fitted parameters of the power law function are compatible within the uncertainties with both data and simulation.

To derive a robust estimate of α, several fits to both data and simulated background events are performed using different analytic functions and looking at different CRs of p_T^{miss}. Within the uncertainties, α is independent of the p_T^{miss} CR used and is consistent between data and simulation. The fitted shape of the low-p_T^{miss} CR in data is taken as
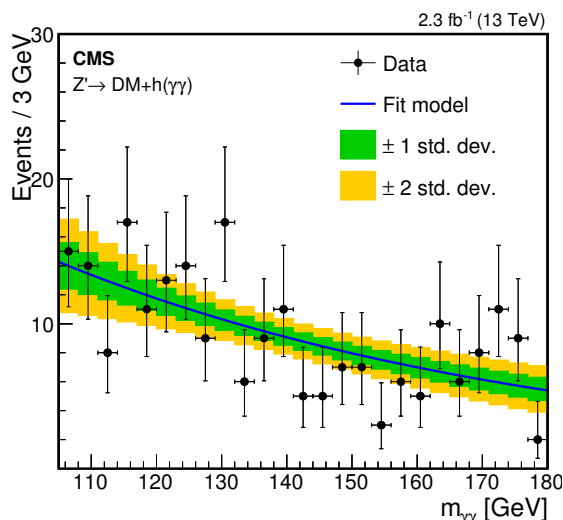
Figure 8. Fit to the diphoton invariant mass distribution in the low-p_T^{miss} CR in data used to evaluate α. The function used is a power law with one free parameter. The uncertainties in the background shapes associated with the statistical uncertainties of the fit are shown by the one and two standard deviation bands.

the nominal background shape. This yields $\alpha = 0.190 \pm 0.035$ (stat). Alternative analytic functions, as well as alternative p_T^{miss} CRs in both data and simulation are considered in order to estimate the systematic uncertainty in this parameter, as described in section 6.

6   Systematic uncertainties

The systematic uncertainties common to the two Higgs boson decay channels are as follows.

An uncertainty of 2.7% is used for the normalization of simulated samples in order to reflect the uncertainty in the integrated luminosity measurement in 2015 [64]. In the h → b$\bar{\text{b}}$ analysis an uncertainty of 2% is estimated in the signal yield for p_T^{miss} above 170 GeV by varying the parameters describing the trigger turn-on. For the h → $\gamma\gamma$ analysis the trigger uncertainty (approximately 1%) is extracted from $Z \to e^+e^-$ events using the tag-and-probe technique [65]. The following uncertainties in clustered and unclustered calorimetric energy affect the p_T^{miss} shapes and the normalization of the signal and background yield predictions: the JES for each jet is varied within one standard deviation as a function of p_T and η, and the efficiency of the event selection is recomputed to assess the variation on the normalization and p_T^{miss} shape for signal and backgrounds; the signal acceptance and efficiency are recomputed after smearing the energy of each jet to correct for the difference in jet energy resolution between the data and simulation ($\approx$5%); the systematic uncertainties in the calibration of unclustered energy in the calorimeter are propagated as normalization and shape uncertainties in the p_T^{miss} calculation. The total effect of the systematic uncertainty in the signal yield, considering all of these variations on p_T^{miss} is approximately 3% for the h → b$\bar{\text{b}}$ analysis and less than 1% for the h → $\gamma\gamma$ analysis. Among the three sources, the JES is the one that most affects the signal yield.

The following systematic uncertainties only affect the h → bb̄ decay channel: the b tagging scale factors are applied consistently to jets in signal and background events. An average systematic uncertainty of 6% per b jet, 12% per c jet, and 15% per light quark or gluon jet is used to account for the normalization uncertainty [50]. The pruned mass distribution of the AK8 jet is not perfectly reproduced by simulation. Therefore, a control region, with a large number of events enriched in boosted hadronically decaying W bosons reconstructed as AK8 jets, is used to measure the systematic uncertainty due to this effect, giving an estimated value of 5%. Moreover, different hadronization algorithms (PYTHIA and HERWIG++) give slightly different shapes for the pruned mass distribution. Therefore, an additional uncertainty of 10% is assigned to account for the difference between simulations. For the boosted regime, the same background normalization scale factor is used for W+jets and top quark backgrounds. The uncertainty in the relative normalization of these two processes is 30%. An uncertainty of 2% is measured by varying the lepton efficiency scale factors within one standard deviation and recomputing the signal selection efficiency. For W+jets, $Z(\to \nu\bar{\nu})$+jets and top quark backgrounds, variations in the renormalization and factorization scales directly affect the normalization and shape of the $p_{\mathrm{T}}^{\mathrm{miss}}$ distribution. A variation of approximately 5% is found for the yields of these backgrounds in the signal region. The uncertainty in the signal acceptance and $p_{\mathrm{T}}^{\mathrm{miss}}$ shape due to the choice of PDFs is measured following the method described by the PDF4LHC group [66]. A variation of approximately 3% is found in the signal yields. The effect of electroweak corrections as described in section 3 is studied by recomputing the normalization and shapes for the W+jets and $Z(\to \nu\bar{\nu})$+jets backgrounds, by alternately removing the corrections or doubling them. An uncertainty of 20% is assumed for the single top quark , SM Higgs boson, and diboson production rates. Uncertainties due to the finite size of the signal and background simulated samples are included in the normalization and shape, such that each bin of the final fitted distributions is affected independently.

In summary, for h → bb̄, the overall uncertainties related to background determination methods, simulation, and theory inputs are estimated to be 10% in the background contributions in the SR. The impact of the uncertainty in the major background contributions (W+jets, $Z(\to \nu\bar{\nu})$+jets and top quarks) in the SR is reduced by constraining the normalizations of these processes in data with the simultaneous fit of $p_{\mathrm{T}}^{\mathrm{miss}}$ shapes in the SR and CRs. The major sources of systematic uncertainties that affect the fit are JES uncertainties, b tagging uncertainties, and the statistical uncertainty in the simulated $Z(\to \nu\bar{\nu})$+jets and W+jets background samples. The effect of the remaining uncertainties on the final fit is ≈1%.

The following systematic uncertainties affect only the h → γγ analysis: as shown in eq. (5.1), the predicted number of nonresonant background events in the SR is evaluated from the number of observed events in the $m_{\gamma\gamma}$ sidebands in the high-$p_{\mathrm{T}}^{\mathrm{miss}}$ region ($N_{\mathrm{SB}}^{\mathrm{bkg}}$) multiplied by a transfer factor α obtained by fitting the $m_{\gamma\gamma}$ distribution in the low-$p_{\mathrm{T}}^{\mathrm{miss}}$ control region. Therefore two different systematic uncertainties are assigned to this procedure, one for $N_{\mathrm{SB}}^{\mathrm{bkg}}$ and one for α. The first systematic uncertainty takes into account the fact that $N_{\mathrm{SB}}^{\mathrm{bkg}}$ is statistically limited. Secondly, a 20% systematic uncertainty is assigned to reflect the imperfect knowledge of the background $m_{\gamma\gamma}$ shape in the low-$p_{\mathrm{T}}^{\mathrm{miss}}$ region, hence

on the knowledge of the α factor. This uncertainty is obtained by performing the fit to the $m_{\gamma\gamma}$ distribution using several analytic functions, using data rather than using simulated events, and using other p_T^{miss} CRs. An observed peak above the diphoton continuum in the $m_{\gamma\gamma}$ distribution around the SM Higgs boson mass would have a SM h $\rightarrow \gamma\gamma$ contribution. In order to extract the DM signal, the resonant background contribution has to be evaluated and subtracted. The SM Higgs boson contribution is affected by both theoretical and experimental systematic uncertainties. For each SM Higgs boson production mechanism (ggh, VBF, tth, Vh), the uncertainties on the PDFs and α_s, provided in ref. [67], are addressed using the procedure from the PDF4LHC group [66]. The size of the systematic uncertainty is computed for each process and category separately by checking the effect of each weight on the final event yield. An additional uncertainty on the h $\rightarrow \gamma\gamma$ branching fraction of 5% is included following ref. [67]. A 1% photon energy scale uncertainty is assigned. This number takes into account the knowledge of the energy scale at the Z boson peak and of its extrapolation to higher masses. The uncertainty on the photon resolution correction factors is evaluated by raising and lowering the estimated additional Gaussian smearing measured at the Z boson peak by 0.5% in quadrature. The photon identification uncertainty is taken as an uncertainty in the data-to-simulation scale factors, which can be as large as 2%, depending on the p_T and the η of the photon.

The h $\rightarrow \gamma\gamma$ decay channel results are only marginally affected by systematic uncertainties as statistical uncertainties dominate the analysis.

7 Results

For the event selection described in section 5, the predicted signal acceptances multiplied by the efficiencies ($A\epsilon$) are listed in table 1 for the two decay channels.

Table 2 shows, for the h $\rightarrow$ b$\bar{\text{b}}$ channel, the SR post-fit yields for each background and signal mass point along with the sum of the statistical and systematic uncertainties for the resolved and boosted regimes. The total background uncertainty is approximately 10% and mainly driven by the systematic uncertainty.

For the h $\rightarrow \gamma\gamma$ channel, when applying the event selection to the data, two events are observed in the $m_{\gamma\gamma}$ sidebands and are used to evaluate the magnitude of the non-resonant background as described in section 5.2.2. This yields an expected number of 0.38 ± 0.27 (stat) nonresonant background events in the SR. Expected resonant background contributions are taken from the simulation as detailed in section 5.2.2 and are 0.057 ± 0.006 (stat) events considering both the Vh production (dominant) and the gluon fusion mode. Zero events are observed in the SR in the data.

Since no excess of events has been observed over the SM background expectation in the signal region, the results of this search are interpreted in terms of an upper limit on the production of DM candidates in association with a Higgs boson in the process Z' $\rightarrow$ Ah $\rightarrow \chi\bar{\chi}$h. The upper limits are computed at 95% confidence level (CL) using a modified frequentist method (CL$_s$) [67–69] computed with an asymptotic approximation [70]. A profile likelihood ratio is used as the test statistic in which systematic uncertainties are modeled as nuisance parameters. These limits are obtained as a function of $m_{Z'}$ and m_A

m_A [GeV]	300	400	500	600	700	800
$m_{Z'}$ [GeV]	h → bb̄					
600	0.058 ± 0.003	0.013 ± 0.003	—	—	—	—
800	0.132 ± 0.003	0.117 ± 0.003	0.083 ± 0.003	0.040 ± 0.003	—	—
1000	0.245 ± 0.004	0.218 ± 0.003	0.167 ± 0.002	0.123 ± 0.003	0.181 ± 0.003	0.066 ± 0.003
1200	0.282 ± 0.003	0.272 ± 0.004	0.262 ± 0.003	0.238 ± 0.004	0.195 ± 0.003	0.126 ± 0.003
1400	0.286 ± 0.003	0.287 ± 0.003	0.283 ± 0.003	0.279 ± 0.003	0.285 ± 0.003	0.249 ± 0.003
1700	0.280 ± 0.003	0.284 ± 0.003	0.283 ± 0.003	0.284 ± 0.003	0.285 ± 0.004	0.284 ± 0.003
2000	0.269 ± 0.005	0.271 ± 0.003	0.275 ± 0.003	0.273 ± 0.003	0.276 ± 0.003	0.279 ± 0.004
2500	0.248 ± 0.003	0.246 ± 0.003	0.250 ± 0.004	0.251 ± 0.003	0.255 ± 0.003	0.256 ± 0.003
$m_{Z'}$ [GeV]	h → γγ					
600	0.317 ± 0.004	0.212 ± 0.003	—	—	—	—
800	0.399 ± 0.004	0.386 ± 0.003	0.348 ± 0.003	0.280 ± 0.003	—	—
1000	0.444 ± 0.004	0.437 ± 0.003	0.422 ± 0.003	0.402 ± 0.003	0.373 ± 0.003	0.330 ± 0.003
1200	0.474 ± 0.004	0.468 ± 0.003	0.461 ± 0.003	0.454 ± 0.003	0.438 ± 0.003	0.417 ± 0.003
1400	0.492 ± 0.004	0.493 ± 0.003	0.485 ± 0.003	0.481 ± 0.003	0.472 ± 0.003	0.465 ± 0.003
1700	0.493 ± 0.004	0.499 ± 0.003	0.504 ± 0.003	0.503 ± 0.003	0.499 ± 0.003	0.498 ± 0.003
2000	0.351 ± 0.004	0.373 ± 0.003	0.394 ± 0.003	0.421 ± 0.003	0.453 ± 0.003	0.488 ± 0.003
2500	0.213 ± 0.004	0.217 ± 0.003	0.227 ± 0.003	0.236 ± 0.003	0.254 ± 0.003	0.268 ± 0.003

Table 1. The product of acceptance and efficiency (with statistical uncertainty) for signal in the SR, after full event selection for the h → bb̄ (upper) and the h → γγ (lower) decay channels. The systematic uncertainty for h → bb̄ (h → γγ) is approximately 10% (5%). For h → bb̄, the value shown here is either for the resolved regime or for the boosted regime, depending on which is used for the calculation of the limit on σ (Z′ → Ah → $\chi\bar{\chi}$h), as shown in figure 10 left.

for both Higgs boson decay channels and for the combination of the two. The two decay channels are combined using the branching ratios predicted by the SM. In the combination of the two analyses, all signal and p_T^{miss}-related systematic uncertainties as well as the systematic uncertainty in the integrated luminosity are assumed to be fully correlated.

Figure 9 (left) shows the 95% CL expected and observed limits on the dark matter production cross section $\sigma(Z' \to Ah \to \chi\bar{\chi}h)$, for h → bb̄ and h → γγ for $m_A = 300\,\text{GeV}$. These results, obtained with $m_\chi = 100\,\text{GeV}$, can be considered valid for any dark matter particle mass below $100\,\text{GeV}$ since the branching fraction for decays of A to DM particles, $\mathcal{B}(A \to \chi\bar{\chi})$, decreases as m_χ increases. As shown in figure 9, for the phase space parameters considered for this model (g_χ and $\tan\beta$ equal to unity), results of the combined analysis are mainly driven by the h → bb̄ channel. The combination with the h → γγ channel provides a 2-4% improvement in terms of constraints on the model for the low Z′ mass values. Future iterations of this search will explore additional phase space regions of the Z′-2HDM model, i.e. larger values of $\tan\beta$, where the h → γγ channel becomes more sensitive than h → bb̄ [7].

h → b$\bar{\text{b}}$ analysis	Number of events (in 2.3 fb^{-1})	
Process	Resolved	Boosted
$Z(\to \nu\bar{\nu})$+jets	$29.6 \pm 2.7 \pm 4.1$	$19.3 \pm 0.8 \pm 1.8$
top quark	$7.3 \pm 1.8 \pm 1.0$	$8.2 \pm 1.7 \pm 1.6$
W+jets	$9.1 \pm 1.6 \pm 1.5$	$10.7 \pm 1.6 \pm 2.0$
Diboson	$2.7 \pm 0.5 \pm 0.5$	$1.5 \pm 0.3 \pm 0.4$
Vh	$2.0 \pm 0.02 \pm 0.2$	$0.8 \pm 0.05 \pm 0.2$
Multijet	$0.01 \pm 0.01 \pm 0.20$	$0.02 \pm 0.01 \pm 0.01$
Total background	$50.7 \pm 2.9 \pm 4.6$	$40.5 \pm 2.4 \pm 3.1$
Data	44	38

$m_{\text{Z}'}$ [GeV]		
600	$29.0 \pm 0.4 \pm 3.5$	—
800	$40.4 \pm 0.5 \pm 3.8$	—
1000	$23.3 \pm 0.3 \pm 2.5$	—
1200	—	$23.6 \pm 0.4 \pm 2.4$
1400	—	$13.1 \pm 0.3 \pm 1.4$
1700	—	$5.6 \pm 0.2 \pm 0.7$
2000	—	$2.3 \pm 0.1 \pm 0.3$
2500	—	$0.24 \pm 0.01 \pm 0.03$

Table 2. Post-fit background event yields and observed numbers of events in data for 2.3 fb^{-1} in both the resolved and the boosted regimes for the h → b$\bar{\text{b}}$ analysis. The expected numbers of signal events for $m_{\text{A}} = 300$ GeV, scaled to the nominal cross section with $g_{\text{Z}'} = 0.8$, are also reported. The statistical and systematic uncertainties are shown separately in that order.

Figures 9 (right) and 10 show the 95% CL expected and observed upper limits on the signal strength $\sigma_{95\%\text{CL}}(\text{Z}' \to \text{Ah} \to \chi\bar{\chi}\text{h})/\sigma_{\text{theory}}(\text{Z}' \to \text{Ah} \to \chi\bar{\chi}\text{h})$. For $m_{\text{A}} = 300$ GeV, the Z' mass range from 600 to 1780 GeV is expected to be excluded with a 95% CL when the signal model cross section is calculated using $g_{\text{Z}'} = 0.8$, while the observed data, for $m_{\text{A}} = 300$ GeV, exclude the Z' mass range from 600 to 1860 GeV. When the signal model cross section is calculated using the constrained $g_{\text{Z}'}$, the expected exclusion range is 830 to 1890 GeV, and the observed exclusion range is 770 to 2040 GeV. Figure 10 shows the expected and observed upper limits on the signal strength for the h → b$\bar{\text{b}}$ and h → $\gamma\gamma$ decay channels. Figure 11 shows the upper limits on the signal strength combining the results from both the h → b$\bar{\text{b}}$ and h → $\gamma\gamma$ decay channels.

8 Summary

A search has been performed for dark matter produced in association with a Higgs boson. The analysis is based on 2.3 fb^{-1} of proton-proton collision data collected by the CMS experiment at $\sqrt{s} = 13$ TeV. This analysis focuses on a Z'-2HDM model in which the Z' decays to a light SM-like scalar Higgs boson and a pseudoscalar boson A, that in turn
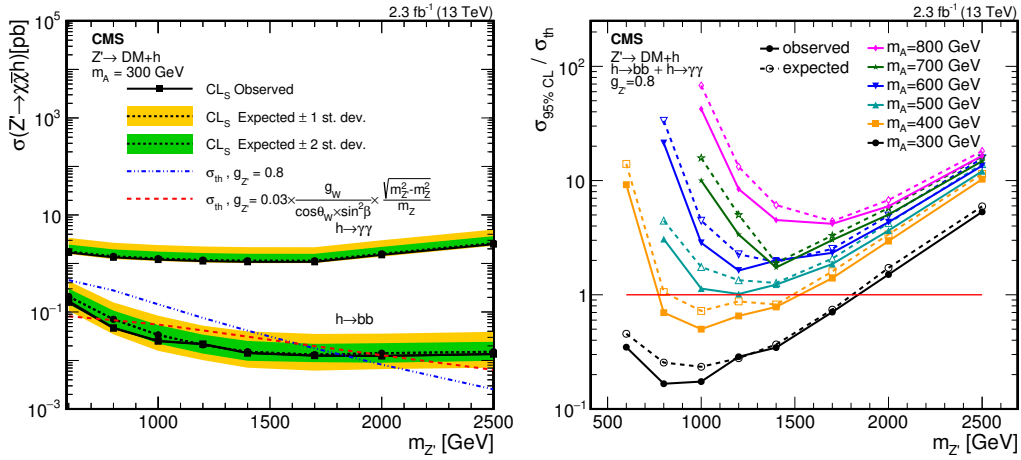
Figure 9. Left: the expected and observed 95% CL limits on dark matter production cross sections for $h \to b\bar{b}$ and $h \to \gamma\gamma$ for $m_A = 300\,\text{GeV}$. The exclusion region is shown for two $g_{Z'}$ values. The dark green and light yellow bands show the 68% and 95% uncertainties on the expected limit. Right: the expected and observed 95% CL limits on the signal strength for $m_A = 300\text{–}800\,\text{GeV}$ are shown. Other parameters for this model are fixed to $m_\chi = 100\,\text{GeV}$ and $\tan\beta = g_\chi = 1$. The theoretical cross section (σ_{th}) used for the right-hand plot is calculated using $g_{Z'} = 0.8$.
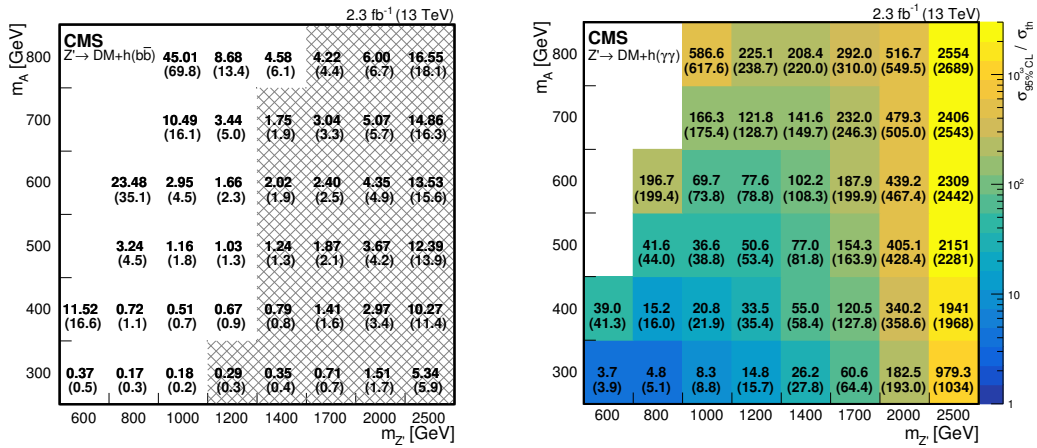
Figure 10. The observed (expected) 95% CL limits on the signal strength (as in figure 9 right), separately for the $h \to b\bar{b}$ (left) and $h \to \gamma\gamma$ (right) decay channels, and for $m_A = 300\text{–}800\,\text{GeV}$ and $m_{Z'} = 600\text{–}2500\,\text{GeV}$. Other parameters for this model are fixed to $m_\chi = 100\,\text{GeV}$ and $\tan\beta = g_\chi = 1$. The theoretical cross sections are calculated using $g_{Z'} = 0.8$. For $h \to b\bar{b}$, the results for the resolved analysis are shown over a white background, whereas the boosted analysis results are shown over a hatched background.
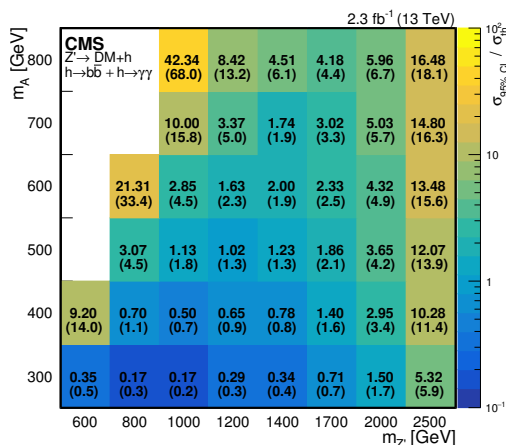
Figure 11. The observed (expected) 95% CL limits on the signal strength (as in figure 9 right) for the combination of h → γγ and h → b$\bar{b}$ decay channels, and for m_A = 300–800 GeV and $m_{Z'}$ = 600–2500 GeV. Other parameters for this model are fixed to m_χ = 100 GeV and $\tan\beta = g_\chi = 1$. The theoretical cross sections times branching fractions are calculated using $g_{Z'}$ = 0.8.

decays to two dark matter candidates. Two distinct channels are studied, where the Higgs boson decays to two b quarks or two photons.

No significant deviation is observed from the standard model background. With optimized selections, limits on the signal cross section $\sigma(Z' \to Ah \to \chi\bar{\chi}h)$ are calculated for various values of $m_{Z'}$ and m_A assuming g_χ and $\tan\beta$ equal to one. The limits are valid for any dark matter particle mass below 100 GeV. For m_A = 300 GeV, the observed data exclude the Z' mass range of 600 to 1860 GeV for $g_{Z'}$ = 0.8, and the range 770 to 2040 GeV for the constrained value of $g_{Z'}$. This is the first result on a search for dark matter produced in association with a Higgs boson at $\sqrt{s}$ = 13 TeV that combines results from the h → b$\bar{b}$ and h → γγ channels.

Acknowledgments

References

[1] G. Bertone, D. Hooper and J. Silk, *Particle dark matter: evidence, candidates and constraints*, *Phys. Rept.* **405** (2005) 279 [`hep-ph/0404175`] [ɪɴSPIRE].

[2] ATLAS collaboration, *Observation of a new particle in the search for the Standard Model Higgs boson with the ATLAS detector at the LHC*, *Phys. Lett.* **B 716** (2012) 1 [`arXiv:1207.7214`] [ɪɴSPIRE].

[3] CMS collaboration, *Observation of a new boson at a mass of 125 GeV with the CMS experiment at the LHC*, *Phys. Lett.* **B 716** (2012) 30 [`arXiv:1207.7235`] [ɪɴSPIRE].

[4] CMS collaboration, *Observation of a new boson with mass near 125 GeV in pp collisions at $\sqrt{s} = 7$ and $8\,TeV$*, *JHEP* **06** (2013) 081 [`arXiv:1303.4571`] [ɪɴSPIRE].

[5] A.A. Petrov and W. Shepherd, *Searching for dark matter at LHC with mono-Higgs production*, *Phys. Lett.* **B 730** (2014) 178 [`arXiv:1311.1511`] [ɪɴSPIRE].

[6] L. Carpenter, A. DiFranzo, M. Mulhearn, C. Shimmin, S. Tulin and D. Whiteson, *Mono-Higgs-boson: A new collider probe of dark matter*, *Phys. Rev.* **D 89** (2014) 075017 [`arXiv:1312.2592`] [ɪɴSPIRE].

[7] A. Berlin, T. Lin and L.-T. Wang, *Mono-Higgs Detection of Dark Matter at the LHC*, *JHEP* **06** (2014) 078 [`arXiv:1402.7074`] [ɪɴSPIRE].

[8] ATLAS collaboration, *Search for dark matter produced in association with a Higgs boson decaying to two bottom quarks in pp collisions at $\sqrt{s} = 8\,TeV$ with the ATLAS detector*, *Phys. Rev.* **D 93** (2016) 072007 [`arXiv:1510.06218`] [ɪɴSPIRE].

[9] ATLAS collaboration, *Search for dark matter in association with a Higgs boson decaying to b-quarks in pp collisions at $\sqrt{s} = 13\,TeV$ with the ATLAS detector*, *Phys. Lett.* **B 765** (2017) 11 [`arXiv:1609.04572`] [ɪɴSPIRE].

[10] ATLAS collaboration, *Search for dark matter in events with missing transverse momentum and a Higgs boson decaying to two photons in pp collisions at $\sqrt{s} = 8\,TeV$ with the ATLAS detector*, *Phys. Rev. Lett.* **115** (2015) 131801 [`arXiv:1506.01081`] [ɪɴSPIRE].

[11] D. Abercrombie et al., *Dark matter benchmark models for early LHC run-2 searches: report of the ATLAS/CMS dark matter forum*, [`arXiv:1507.00966`] [ɪɴSPIRE].

[12] T.D. Lee, *A theory of spontaneous T violation*, *Phys. Rev.* **D 8** (1973) 1226 [INSPIRE].

[13] G.C. Branco, P.M. Ferreira, L. Lavoura, M.N. Rebelo, M. Sher and J.P. Silva, *Theory and phenomenology of two-Higgs-doublet models*, *Phys. Rept.* **516** (2012) 1 [arXiv:1106.0034] [INSPIRE].

[14] N. Craig, J. Galloway and S. Thomas, *Searching for Signs of the Second Higgs Doublet*, arXiv:1305.2424 [INSPIRE].

[15] CMS collaboration, *The CMS experiment at the CERN LHC*, 2008 *JINST* **3** S08004 [INSPIRE].

[16] J. Alwall et al., *The automated computation of tree-level and next-to-leading order differential cross sections and their matching to parton shower simulations*, *JHEP* **07** (2014) 079 [arXiv:1405.0301] [INSPIRE].

[17] T. Sjöstrand et al., *An introduction to PYTHIA 8.2*, *Comput. Phys. Commun.* **191** (2015) 159 [arXiv:1410.3012] [INSPIRE].

[18] C. Oleari, *The POWHEG-BOX*, *Nucl. Phys. Proc. Suppl.* **205-206** (2010) 36 [arXiv:1007.3893] [INSPIRE].

[19] G. Luisoni, P. Nason, C. Oleari and F. Tramontano, $HW^{\pm}/HZ + 0$ *and* 1 *jet at NLO with the POWHEG BOX interfaced to GoSam and their merging within MiNLO*, *JHEP* **10** (2013) 083 [arXiv:1306.2542] [INSPIRE].

[20] P. Nason and C. Oleari, *NLO Higgs boson production via vector-boson fusion matched with shower in POWHEG*, *JHEP* **02** (2010) 037 [arXiv:0911.5299] [INSPIRE].

[21] P. Nason, *A new method for combining NLO QCD with shower Monte Carlo algorithms*, *JHEP* **11** (2004) 040 [hep-ph/0409146] [INSPIRE].

[22] S. Frixione, P. Nason and C. Oleari, *Matching NLO QCD computations with Parton Shower simulations: the POWHEG method*, *JHEP* **11** (2007) 070 [arXiv:0709.2092] [INSPIRE].

[23] S. Alioli, P. Nason, C. Oleari and E. Re, *A general framework for implementing NLO calculations in shower Monte Carlo programs: the POWHEG BOX*, *JHEP* **06** (2010) 043 [arXiv:1002.2581] [INSPIRE].

[24] S. Frixione, P. Nason and G. Ridolfi, *A positive-weight next-to-leading-order Monte Carlo for heavy flavour hadroproduction*, *JHEP* **09** (2007) 126 [arXiv:0707.3088] [INSPIRE].

[25] E. Re, *Single-top Wt-channel production matched with parton showers using the POWHEG method*, *Eur. Phys. J.* **C 71** (2011) 1547 [arXiv:1009.2450] [INSPIRE].

[26] CMS collaboration, *Measurement of differential top-quark pair production cross sections in pp colisions at* $\sqrt{s} = 7$ *TeV*, *Eur. Phys. J.* **C 73** (2013) 2339 [arXiv:1211.2220] [INSPIRE].

[27] CMS collaboration, *Measurement of the differential cross section for top quark pair production in pp collisions at* $\sqrt{s} = 8$ *TeV*, *Eur. Phys. J.* **C 75** (2015) 542 [arXiv:1505.04480] [INSPIRE].

[28] M.L. Mangano, M. Moretti, F. Piccinini and M. Treccani, *Matching matrix elements and shower evolution for top-quark production in hadronic collisions*, *JHEP* **01** (2007) 013 [hep-ph/0611129] [INSPIRE].

[29] Y. Li and F. Petriello, *Combining QCD and electroweak corrections to dilepton production in the framework of FEWZ simulation code*, *Phys. Rev.* **D 86** (2012) 094034 [arXiv:1208.5967] [INSPIRE].

[30] J.H. Kuhn, A. Kulesza, S. Pozzorini and M. Schulze, *Electroweak corrections to hadronic photon production at large transverse momenta*, *JHEP* **03** (2006) 059 [hep-ph/0508253] [INSPIRE].

[31] S. Kallweit, J.M. Lindert, P. Maierhöfer, S. Pozzorini and M. Schönherr, *NLO electroweak automation and precise predictions for W+multijet production at the LHC*, *JHEP* **04** (2015) 012 [arXiv:1412.5157] [INSPIRE].

[32] S. Kallweit, J.M. Lindert, P. Maierhöfer, S. Pozzorini and M. Schönherr, *NLO QCD+EW predictions for V + jets including off-shell vector-boson decays and multijet merging*, *JHEP* **04** (2016) 021 [arXiv:1511.08692] [INSPIRE].

[33] P. Nason and G. Zanderighi, W^+W^- , WZ and ZZ production in the POWHEG-BOX-V2, *Eur. Phys. J.* **C 74** (2014) 2702 [arXiv:1311.1365] [INSPIRE].

[34] NNPDF collaboration, R.D. Ball et al., *Parton distributions for the LHC Run II*, *JHEP* **04** (2015) 040 [arXiv:1410.8849] [INSPIRE].

[35] P. Skands, S. Carrazza and J. Rojo, *Tuning PYTHIA 8.1: the Monash 2013 Tune*, *Eur. Phys. J.* **C 74** (2014) 3024 [arXiv:1404.5630] [INSPIRE].

[36] CMS collaboration, *Event generator tunes obtained from underlying event and multiparton scattering measurements*, *Eur. Phys. J.* **C 76** (2016) 155 [arXiv:1512.00815] [INSPIRE].

[37] M. Bahr et al., *HERWIG++ physics and manual*, *Eur. Phys. J.* **C 58** (2008) 639 [arXiv:0803.0883] [INSPIRE].

[38] S. Gieseke, C. Rohr and A. Siodmok, *Colour reconnections in HERWIG++*, *Eur. Phys. J.* **C 72** (2012) 2225 [arXiv:1206.0041] [INSPIRE].

[39] M.H. Seymour and A. Siodmok, *Constraining MPI models using σ_{eff} and recent Tevatron and LHC underlying event data*, *JHEP* **10** (2013) 113 [arXiv:1307.5015] [INSPIRE].

[40] GEANT4 collaboration, S. Agostinelli et al., *GEANT4: A simulation toolkit*, *Nucl. Instrum. Meth.* **A 506** (2003) 250 [INSPIRE].

[41] CMS collaboration, *Particle-Flow Event Reconstruction in CMS and Performance for Jets, Taus and MET*, CMS-PAS-PFT-09-001 (2009).

[42] CMS collaboration, *Commissioning of the Particle-flow Event Reconstruction with the first LHC collisions recorded in the CMS detector*, CMS-PAS-PFT-10-001 (2010).

[43] CMS collaboration, *Particle-flow reconstruction and global event description with the CMS detector*, 2017 *JINST* **12** P10003 [arXiv:1706.04965] [INSPIRE].

[44] M. Cacciari, G.P. Salam and G. Soyez, *The anti-k_t jet clustering algorithm*, *JHEP* **04** (2008) 063 [arXiv:0802.1189] [INSPIRE].

[45] M. Cacciari, G.P. Salam and G. Soyez, *FastJet user manual*, *Eur. Phys. J.* **C 72** (2012) 1896 [arXiv:1111.6097] [INSPIRE].

[46] S.D. Ellis, C.K. Vermilion and J.R. Walsh, *Techniques for improved heavy particle searches with jet substructure*, *Phys. Rev.* **D 80** (2009) 051501 [arXiv:0903.5081] [INSPIRE].

[47] S.D. Ellis, C.K. Vermilion and J.R. Walsh, *Recombination algorithms and jet substructure: pruning as a tool for heavy particle searches*, *Phys. Rev.* **D 81** (2010) 094023 [arXiv:0912.0033] [INSPIRE].

[48] CMS collaboration, *Jet energy scale and resolution in the CMS experiment in pp collisions at 8 TeV*, 2017 *JINST* **12** P02014 [arXiv:1607.03663] [INSPIRE].

[49] CMS collaboration, *Performance of missing energy reconstruction in 13 TeV pp collision data using the CMS detector*, CMS-PAS-JME-16-004 (2016).

[50] CMS collaboration, *Identification of b quark jets at the CMS Experiment in the LHC Run 2*, CMS-PAS-BTV-15-001 (2016).

[51] CMS collaboration, *Identification of b-quark jets with the CMS experiment*, 2013 *JINST* **8** P04013 [arXiv:1211.4462] [ɪɴSPIRE].

[52] M. Dasgupta, A. Fregoso, S. Marzani and G.P. Salam, *Towards an understanding of jet substructure*, *JHEP* **09** (2013) 029 [arXiv:1307.0007] [ɪɴSPIRE].

[53] A.J. Larkoski, S. Marzani, G. Soyez and J. Thaler, *Soft drop*, *JHEP* **05** (2014) 146 [arXiv:1402.2657] [ɪɴSPIRE].

[54] CMS collaboration, *CMS technical design report, volume II: Physics performance*, *J. Phys.* **G 34** (2007) 995 [ɪɴSPIRE].

[55] CMS collaboration, *Performance of photon reconstruction and identification with the CMS detector in proton-proton collisions at $\sqrt{s} = 8$ TeV*, 2015 *JINST* **10** P08010 [arXiv:1502.02702] [ɪɴSPIRE].

[56] CMS collaboration, *Performance of electron reconstruction and selection with the CMS detector in proton-proton collisions at $\sqrt{s} = 8$ TeV*, 2015 *JINST* **10** P06005 [arXiv:1502.02701] [ɪɴSPIRE].

[57] CMS collaboration, *Performance of CMS muon reconstruction in pp collision events at $\sqrt{s} = 7$ TeV*, 2012 *JINST* **7** P10002 [arXiv:1206.4071] [ɪɴSPIRE].

[58] CMS collaboration, *Reconstruction and identification of τ lepton decays to hadrons and ν_τ at CMS*, 2016 *JINST* **11** P01019 [arXiv:1510.07488] [ɪɴSPIRE].

[59] CMS collaboration, *The performance of the CMS muon detector in proton-proton collisions at $\sqrt{s} = 7$ TeV at the LHC*, 2013 *JINST* **8** P11002 [arXiv:1306.6905] [ɪɴSPIRE].

[60] M. Cacciari and G.P. Salam, *Pileup subtraction using jet areas*, *Phys. Lett.* **B 659** (2008) 119 [arXiv:0707.1378] [ɪɴSPIRE].

[61] CMS collaboration, *Measurement of differential cross sections for Higgs boson production in the diphoton decay channel in pp collisions at $\sqrt{s} = 8$ TeV*, *Eur. Phys. J.* **C 76** (2016) 13 [arXiv:1508.07819] [ɪɴSPIRE].

[62] CMS collaboration, *Observation of the diphoton decay of the Higgs boson and measurement of its properties*, *Eur. Phys. J.* **C 74** (2014) 3076 [arXiv:1407.0558] [ɪɴSPIRE].

[63] CMS collaboration, *Search for resonant production of high-mass photon pairs in proton-proton collisions at $\sqrt{s} = 8$ and 13 TeV*, *Phys. Rev. Lett.* **117** (2016) 051802 [arXiv:1606.04093] [ɪɴSPIRE].

[64] CMS collaboration, *CMS luminosity measurement for the 2015 data-taking period*, CMS-PAS-LUM-15-001 (2016).

[65] CMS collaboration, *Measurements of inclusive W and Z cross sections in pp collisions at $\sqrt{s} = 7$ TeV*, *JHEP* **01** (2011) 080 [arXiv:1012.2466] [ɪɴSPIRE].

[66] J. Butterworth et al., *PDF4LHC recommendations for LHC Run II*, *J. Phys.* **G 43** (2016) 023001 [arXiv:1510.03865] [ɪɴSPIRE].

[67] LHC Higgs Cross section Working Group collaboration, J.R. Andersen et al., *Handbook of LHC Higgs cross sections: 3. Higgs properties: report of the LHC Higgs cross section working group*, arXiv:1307.1347 [INSPIRE].

[68] A.L. Read, *Presentation of search results: The CL(s) technique*, *J. Phys.* **G 28** (2002) 2693 [INSPIRE].

[69] T. Junk, *Confidence level computation for combining searches with small statistics*, *Nucl. Instrum. Meth.* **A 434** (1999) 435 [hep-ex/9902006] [INSPIRE].

[70] G. Cowan, K. Cranmer, E. Gross and O. Vitells, *Asymptotic formulae for likelihood-based tests of new physics*, *Eur. Phys. J.* **C 71** (2011) 1554 [*Erratum ibid.* **C 73** (2013) 2501] [arXiv:1007.1727] [INSPIRE].

The CMS collaboration

Yerevan Physics Institute, Yerevan, Armenia

A.M. Sirunyan, A. Tumasyan

Institut für Hochenergiephysik, Wien, Austria

W. Adam, E. Asilar, T. Bergauer, J. Brandstetter, E. Brondolin, M. Dragicevic, J. Erö, M. Flechl, M. Friedl, R. Frühwirth[1], V.M. Ghete, C. Hartl, N. Hörmann, J. Hrubec, M. Jeitler[1], A. König, I. Krätschmer, D. Liko, T. Matsushita, I. Mikulec, D. Rabady, N. Rad, B. Rahbaran, H. Rohringer, J. Schieck[1], J. Strauss, W. Waltenberger, C.-E. Wulz[1]

Institute for Nuclear Problems, Minsk, Belarus

O. Dvornikov, V. Makarenko, V. Mossolov, J. Suarez Gonzalez, V. Zykunov

National Centre for Particle and High Energy Physics, Minsk, Belarus

N. Shumeiko

Universiteit Antwerpen, Antwerpen, Belgium

S. Alderweireldt, E.A. De Wolf, X. Janssen, J. Lauwers, M. Van De Klundert, H. Van Haevermaet, P. Van Mechelen, N. Van Remortel, A. Van Spilbeeck

Vrije Universiteit Brussel, Brussel, Belgium

S. Abu Zeid, F. Blekman, J. D'Hondt, N. Daci, I. De Bruyn, K. Deroover, S. Lowette, S. Moortgat, L. Moreels, A. Olbrechts, Q. Python, K. Skovpen, S. Tavernier, W. Van Doninck, P. Van Mulders, I. Van Parijs

Université Libre de Bruxelles, Bruxelles, Belgium

H. Brun, B. Clerbaux, G. De Lentdecker, H. Delannoy, G. Fasanella, L. Favart, R. Goldouzian, A. Grebenyuk, G. Karapostoli, T. Lenzi, A. Léonard, J. Luetic, T. Maerschalk, A. Marinov, A. Randle-conde, T. Seva, C. Vander Velde, P. Vanlaer, D. Vannerom, R. Yonamine, F. Zenoni, F. Zhang[2]

Ghent University, Ghent, Belgium

T. Cornelis, D. Dobur, A. Fagot, M. Gul, I. Khvastunov, D. Poyraz, S. Salva, R. Schöfbeck, M. Tytgat, W. Van Driessche, E. Yazgan, N. Zaganidis

Université Catholique de Louvain, Louvain-la-Neuve, Belgium

H. Bakhshiansohi, O. Bondu, S. Brochet, G. Bruno, A. Caudron, S. De Visscher, C. Delaere, M. Delcourt, B. Francois, A. Giammanco, A. Jafari, M. Komm, G. Krintiras, V. Lemaitre, A. Magitteri, A. Mertens, M. Musich, K. Piotrzkowski, L. Quertenmont, M. Selvaggi, M. Vidal Marono, S. Wertz

Université de Mons, Mons, Belgium

N. Beliy

Centro Brasileiro de Pesquisas Fisicas, Rio de Janeiro, Brazil

W.L. Aldá Júnior, F.L. Alves, G.A. Alves, L. Brito, C. Hensel, A. Moraes, M.E. Pol, P. Rebello Teles

Universidade do Estado do Rio de Janeiro, Rio de Janeiro, Brazil

E. Belchior Batista Das Chagas, W. Carvalho, J. Chinellato[3], A. Custódio, E.M. Da Costa, G.G. Da Silveira[4], D. De Jesus Damiao, C. De Oliveira Martins, S. Fonseca De Souza, L.M. Huertas Guativa, H. Malbouisson, D. Matos Figueiredo, C. Mora Herrera, L. Mundim, H. Nogima, W.L. Prado Da Silva, A. Santoro, A. Sznajder, E.J. Tonelli Manganote[3], F. Torres Da Silva De Araujo, A. Vilela Pereira

Universidade Estadual Paulista[a], Universidade Federal do ABC[b], São Paulo, Brazil

S. Ahuja[a], C.A. Bernardes[a], S. Dogra[a], T.R. Fernandez Perez Tomei[a], E.M. Gregores[b], P.G. Mercadante[b], C.S. Moon[a], S.F. Novaes[a], Sandra S. Padula[a], D. Romero Abad[b], J.C. Ruiz Vargas[a]

Institute for Nuclear Research and Nuclear Energy, Sofia, Bulgaria

A. Aleksandrov, R. Hadjiiska, P. Iaydjiev, M. Rodozov, S. Stoykova, G. Sultanov, M. Vutova

University of Sofia, Sofia, Bulgaria

A. Dimitrov, I. Glushkov, L. Litov, B. Pavlov, P. Petkov

Beihang University, Beijing, China

W. Fang[5]

Institute of High Energy Physics, Beijing, China

M. Ahmad, J.G. Bian, G.M. Chen, H.S. Chen, M. Chen, Y. Chen, T. Cheng, C.H. Jiang, D. Leggat, Z. Liu, F. Romeo, M. Ruan, S.M. Shaheen, A. Spiezia, J. Tao, C. Wang, Z. Wang, H. Zhang, J. Zhao

State Key Laboratory of Nuclear Physics and Technology, Peking University, Beijing, China

Y. Ban, G. Chen, Q. Li, S. Liu, Y. Mao, S.J. Qian, D. Wang, Z. Xu

Universidad de Los Andes, Bogota, Colombia

C. Avila, A. Cabrera, L.F. Chaparro Sierra, C. Florez, J.P. Gomez, C.F. González Hernández, J.D. Ruiz Alvarez[6], J.C. Sanabria

University of Split, Faculty of Electrical Engineering, Mechanical Engineering and Naval Architecture, Split, Croatia

N. Godinovic, D. Lelas, I. Puljak, P.M. Ribeiro Cipriano, T. Sculac

University of Split, Faculty of Science, Split, Croatia

Z. Antunovic, M. Kovac

Institute Rudjer Boskovic, Zagreb, Croatia

V. Brigljevic, D. Ferencek, K. Kadija, B. Mesic, T. Susa

University of Cyprus, Nicosia, Cyprus

M.W. Ather, A. Attikis, G. Mavromanolakis, J. Mousa, C. Nicolaou, F. Ptochos, P.A. Razis, H. Rykaczewski

Charles University, Prague, Czech Republic

M. Finger[7], M. Finger Jr.[7]

Universidad San Francisco de Quito, Quito, Ecuador

E. Carrera Jarrin

Academy of Scientific Research and Technology of the Arab Republic of Egypt, Egyptian Network of High Energy Physics, Cairo, Egypt

A.A. Abdelalim[8,9], Y. Mohammed[10], E. Salama[11,12]

National Institute of Chemical Physics and Biophysics, Tallinn, Estonia

M. Kadastik, L. Perrini, M. Raidal, A. Tiko, C. Veelken

Department of Physics, University of Helsinki, Helsinki, Finland

P. Eerola, J. Pekkanen, M. Voutilainen

Helsinki Institute of Physics, Helsinki, Finland

J. Härkönen, T. Järvinen, V. Karimäki, R. Kinnunen, T. Lampén, K. Lassila-Perini, S. Lehti, T. Lindén, P. Luukka, J. Tuominiemi, E. Tuovinen, L. Wendland

Lappeenranta University of Technology, Lappeenranta, Finland

J. Talvitie, T. Tuuva

IRFU, CEA, Université Paris-Saclay, Gif-sur-Yvette, France

M. Besancon, F. Couderc, M. Dejardin, D. Denegri, B. Fabbro, J.L. Faure, C. Favaro, F. Ferri, S. Ganjour, S. Ghosh, A. Givernaud, P. Gras, G. Hamel de Monchenault, P. Jarry, I. Kucher, E. Locci, M. Machet, J. Malcles, J. Rander, A. Rosowsky, M. Titov

Laboratoire Leprince-Ringuet, Ecole Polytechnique, IN2P3-CNRS, Palaiseau, France

A. Abdulsalam, C. Amendola, I. Antropov, S. Baffioni, F. Beaudette, P. Busson, L. Cadamuro, E. Chapon, C. Charlot, O. Davignon, R. Granier de Cassagnac, M. Jo, S. Lisniak, P. Miné, M. Nguyen, C. Ochando, G. Ortona, P. Paganini, P. Pigard, S. Regnard, R. Salerno, Y. Sirois, A.G. Stahl Leiton, T. Strebler, Y. Yilmaz, A. Zabi, A. Zghiche

Institut Pluridisciplinaire Hubert Curien (IPHC), Université de Strasbourg, CNRS-IN2P3

J.-L. Agram[13], J. Andrea, D. Bloch, J.-M. Brom, M. Buttignol, E.C. Chabert, N. Chanon, C. Collard, E. Conte[13], X. Coubez, J.-C. Fontaine[13], D. Gelé, U. Goerlach, A.-C. Le Bihan, P. Van Hove

Centre de Calcul de l'Institut National de Physique Nucleaire et de Physique des Particules, CNRS/IN2P3, Villeurbanne, France

S. Gadrat

Université de Lyon, Université Claude Bernard Lyon 1, CNRS-IN2P3, Institut de Physique Nucléaire de Lyon, Villeurbanne, France

S. Beauceron, C. Bernet, G. Boudoul, C.A. Carrillo Montoya, R. Chierici, D. Contardo, B. Courbon, P. Depasse, H. El Mamouni, J. Fay, S. Gascon, M. Gouzevitch, G. Grenier, B. Ille, F. Lagarde, I.B. Laktineh, M. Lethuillier, L. Mirabito, A.L. Pequegnot, S. Perries, A. Popov[14], V. Sordini, M. Vander Donckt, P. Verdier, S. Viret

Georgian Technical University, Tbilisi, Georgia

T. Toriashvili[15]

Tbilisi State University, Tbilisi, Georgia

Z. Tsamalaidze[7]

RWTH Aachen University, I. Physikalisches Institut, Aachen, Germany

C. Autermann, S. Beranek, L. Feld, M.K. Kiesel, K. Klein, M. Lipinski, M. Preuten, C. Schomakers, J. Schulz, T. Verlage

RWTH Aachen University, III. Physikalisches Institut A, Aachen, Germany

A. Albert, M. Brodski, E. Dietz-Laursonn, D. Duchardt, M. Endres, M. Erdmann, S. Erdweg, T. Esch, R. Fischer, A. Güth, M. Hamer, T. Hebbeker, C. Heidemann, K. Hoepfner, S. Knutzen, M. Merschmeyer, A. Meyer, P. Millet, S. Mukherjee, M. Olschewski, K. Padeken, T. Pook, M. Radziej, H. Reithler, M. Rieger, F. Scheuch, L. Sonnenschein, D. Teyssier, S. Thüer

RWTH Aachen University, III. Physikalisches Institut B, Aachen, Germany

V. Cherepanov, G. Flügge, B. Kargoll, T. Kress, A. Künsken, J. Lingemann, T. Müller, A. Nehrkorn, A. Nowack, C. Pistone, O. Pooth, A. Stahl[16]

Deutsches Elektronen-Synchrotron, Hamburg, Germany

M. Aldaya Martin, T. Arndt, C. Asawatangtrakuldee, K. Beernaert, O. Behnke, U. Behrens, A.A. Bin Anuar, K. Borras[17], A. Campbell, P. Connor, C. Contreras-Campana, F. Costanza, C. Diez Pardos, G. Dolinska, G. Eckerlin, D. Eckstein, T. Eichhorn, E. Eren, E. Gallo[18], J. Garay Garcia, A. Geiser, A. Gizhko, J.M. Grados Luyando, A. Grohsjean, P. Gunnellini, A. Harb, J. Hauk, M. Hempel[19], H. Jung, A. Kalogeropoulos, O. Karacheban[19], M. Kasemann, J. Keaveney, C. Kleinwort, I. Korol, D. Krücker, W. Lange, A. Lelek, T. Lenz, J. Leonard, K. Lipka, A. Lobanov, W. Lohmann[19], R. Mankel, I.-A. Melzer-Pellmann, A.B. Meyer, G. Mittag, J. Mnich, A. Mussgiller, D. Pitzl, R. Placakyte, A. Raspereza, B. Roland, M.Ö. Sahin, P. Saxena, T. Schoerner-Sadenius, S. Spannagel, N. Stefaniuk, G.P. Van Onsem, R. Walsh, C. Wissing

University of Hamburg, Hamburg, Germany

V. Blobel, M. Centis Vignali, A.R. Draeger, T. Dreyer, E. Garutti, D. Gonzalez, J. Haller, M. Hoffmann, A. Junkes, R. Klanner, R. Kogler, N. Kovalchuk, S. Kurz, T. Lapsien, I. Marchesini, D. Marconi, M. Meyer, M. Niedziela, D. Nowatschin, F. Pantaleo[16], T. Peiffer, A. Perieanu, C. Scharf, P. Schleper, A. Schmidt, S. Schumann, J. Schwandt, J. Sonneveld, H. Stadie, G. Steinbrück, F.M. Stober, M. Stöver, H. Tholen, D. Troendle, E. Usai, L. Vanelderen, A. Vanhoefer, B. Vormwald

Institut für Experimentelle Kernphysik, Karlsruhe, Germany

M. Akbiyik, C. Barth, S. Baur, C. Baus, J. Berger, E. Butz, R. Caspart, T. Chwalek, F. Colombo, W. De Boer, A. Dierlamm, S. Fink, B. Freund, R. Friese, M. Giffels, A. Gilbert, P. Goldenzweig, D. Haitz, F. Hartmann[16], S.M. Heindl, U. Husemann, F. Kassel[16], I. Katkov[14], S. Kudella, H. Mildner, M.U. Mozer, Th. Müller, M. Plagge, G. Quast, K. Rabbertz, S. Röcker, F. Roscher, M. Schröder, I. Shvetsov, G. Sieber, H.J. Simonis, R. Ulrich, S. Wayand, M. Weber, T. Weiler, S. Williamson, C. Wöhrmann, R. Wolf

Institute of Nuclear and Particle Physics (INPP), NCSR Demokritos, Aghia Paraskevi, Greece

G. Anagnostou, G. Daskalakis, T. Geralis, V.A. Giakoumopoulou, A. Kyriakis, D. Loukas, I. Topsis-Giotis

National and Kapodistrian University of Athens, Athens, Greece

S. Kesisoglou, A. Panagiotou, N. Saoulidou, E. Tziaferi

University of Ioánnina, Ioánnina, Greece

I. Evangelou, G. Flouris, C. Foudas, P. Kokkas, N. Loukas, N. Manthos, I. Papadopoulos, E. Paradas

MTA-ELTE Lendület CMS Particle and Nuclear Physics Group, Eötvös Loránd University, Budapest, Hungary

N. Filipovic, G. Pasztor

Wigner Research Centre for Physics, Budapest, Hungary

G. Bencze, C. Hajdu, D. Horvath[20], F. Sikler, V. Veszpremi, G. Vesztergombi[21], A.J. Zsigmond

Institute of Nuclear Research ATOMKI, Debrecen, Hungary

N. Beni, S. Czellar, J. Karancsi[22], A. Makovec, J. Molnar, Z. Szillasi

Institute of Physics, University of Debrecen

M. Bartók[21], P. Raics, Z.L. Trocsanyi, B. Ujvari

Indian Institute of Science (IISc)

S. Choudhury, J.R. Komaragiri

National Institute of Science Education and Research, Bhubaneswar, India

S. Bahinipati[23], S. Bhowmik[24], P. Mal, K. Mandal, A. Nayak[25], D.K. Sahoo[23], N. Sahoo, S.K. Swain

Panjab University, Chandigarh, India

S. Bansal, S.B. Beri, V. Bhatnagar, R. Chawla, U.Bhawandeep, A.K. Kalsi, A. Kaur, M. Kaur, R. Kumar, P. Kumari, A. Mehta, M. Mittal, J.B. Singh, G. Walia

University of Delhi, Delhi, India

Ashok Kumar, A. Bhardwaj, B.C. Choudhary, R.B. Garg, S. Keshri, A. Kumar, S. Malhotra, M. Naimuddin, K. Ranjan, R. Sharma, V. Sharma

Saha Institute of Nuclear Physics, Kolkata, India

R. Bhattacharya, S. Bhattacharya, K. Chatterjee, S. Dey, S. Dutt, S. Dutta, S. Ghosh, N. Majumdar, A. Modak, K. Mondal, S. Mukhopadhyay, S. Nandan, A. Purohit, A. Roy, D. Roy, S. Roy Chowdhury, S. Sarkar, M. Sharan, S. Thakur

Indian Institute of Technology Madras, Madras, India

P.K. Behera

Bhabha Atomic Research Centre, Mumbai, India

R. Chudasama, D. Dutta, V. Jha, V. Kumar, A.K. Mohanty[16], P.K. Netrakanti, L.M. Pant, P. Shukla, A. Topkar

Tata Institute of Fundamental Research-A, Mumbai, India

T. Aziz, S. Dugad, G. Kole, B. Mahakud, S. Mitra, G.B. Mohanty, B. Parida, N. Sur, B. Sutar

Tata Institute of Fundamental Research-B, Mumbai, India

S. Banerjee, R.K. Dewanjee, S. Ganguly, M. Guchait, Sa. Jain, S. Kumar, M. Maity[24], G. Majumder, K. Mazumdar, T. Sarkar[24], N. Wickramage[26]

Indian Institute of Science Education and Research (IISER), Pune, India

S. Chauhan, S. Dube, V. Hegde, A. Kapoor, K. Kothekar, S. Pandey, A. Rane, S. Sharma

Institute for Research in Fundamental Sciences (IPM), Tehran, Iran

S. Chenarani[27], E. Eskandari Tadavani, S.M. Etesami[27], M. Khakzad, M. Mohammadi Najafabadi, M. Naseri, S. Paktinat Mehdiabadi[28], F. Rezaei Hosseinabadi, B. Safarzadeh[29], M. Zeinali

University College Dublin, Dublin, Ireland

M. Felcini, M. Grunewald

INFN Sezione di Bari^a, Università di Bari^b, Politecnico di Bari^c, Bari, Italy

M. Abbrescia^{a,b}, C. Calabria^{a,b}, C. Caputo^{a,b}, A. Colaleo^a, D. Creanza^{a,c}, L. Cristella^{a,b}, N. De Filippis^{a,c}, M. De Palma^{a,b}, L. Fiore^a, G. Iaselli^{a,c}, G. Maggi^{a,c}, M. Maggi^a, G. Miniello^{a,b}, S. My^{a,b}, S. Nuzzo^{a,b}, A. Pompili^{a,b}, G. Pugliese^{a,c}, R. Radogna^{a,b}, A. Ranieri^a, G. Selvaggi^{a,b}, A. Sharma^a, L. Silvestris^{a,16}, R. Venditti^{a,b}, P. Verwilligen^a

INFN Sezione di Bologna^a, Università di Bologna^b, Bologna, Italy

G. Abbiendi^a, C. Battilana, D. Bonacorsi^{a,b}, S. Braibant-Giacomelli^{a,b}, L. Brigliadori^{a,b}, R. Campanini^{a,b}, P. Capiluppi^{a,b}, A. Castro^{a,b}, F.R. Cavallo^a, S.S. Chhibra^{a,b}, G. Codispoti^{a,b}, M. Cuffiani^{a,b}, G.M. Dallavalle^a, F. Fabbri^a, A. Fanfani^{a,b}, D. Fasanella^{a,b}, P. Giacomelli^a, C. Grandi^a, L. Guiducci^{a,b}, S. Marcellini^a, G. Masetti^a, A. Montanari^a, F.L. Navarria^{a,b}, A. Perrotta^a, A.M. Rossi^{a,b}, T. Rovelli^{a,b}, G.P. Siroli^{a,b}, N. Tosi^{a,b,16}

INFN Sezione di Catania^a, Università di Catania^b, Catania, Italy

S. Albergo^{a,b}, S. Costa^{a,b}, A. Di Mattia^a, F. Giordano^{a,b}, R. Potenza^{a,b}, A. Tricomi^{a,b}, C. Tuve^{a,b}

INFN Sezione di Firenze^a, Università di Firenze^b, Firenze, Italy

G. Barbagli^a, V. Ciulli^{a,b}, C. Civinini^a, R. D'Alessandro^{a,b}, E. Focardi^{a,b}, P. Lenzi^{a,b}, M. Meschini^a, S. Paoletti^a, L. Russo^{a,30}, G. Sguazzoni^a, D. Strom^a, L. Viliani^{a,b,16}

INFN Laboratori Nazionali di Frascati, Frascati, Italy

L. Benussi, S. Bianco, F. Fabbri, D. Piccolo, F. Primavera^{16}

INFN Sezione di Genova^a, Università di Genova^b, Genova, Italy

V. Calvelli^{a,b}, F. Ferro^a, M.R. Monge^{a,b}, E. Robutti^a, S. Tosi^{a,b}

INFN Sezione di Milano-Bicocca^a, Università di Milano-Bicocca^b, Milano, Italy

L. Brianza^{a,b,16}, F. Brivio^{a,b}, V. Ciriolo, M.E. Dinardo^{a,b}, S. Fiorendi^{a,b,16}, S. Gennai^a, A. Ghezzi^{a,b}, P. Govoni^{a,b}, M. Malberti^{a,b}, S. Malvezzi^a, R.A. Manzoni^{a,b}, D. Menasce^a, L. Moroni^a, M. Paganoni^{a,b}, D. Pedrini^a, S. Pigazzini^{a,b}, S. Ragazzi^{a,b}, T. Tabarelli de Fatis^{a,b}

INFN Sezione di Napoli^a, Università di Napoli 'Federico II'^{b}, Napoli, Italy, Università della Basilicata^c, Potenza, Italy, Università G. Marconi^d, Roma, Italy

S. Buontempo^a, N. Cavallo^{a,c}, G. De Nardo, S. Di Guida^{a,d,16}, M. Esposito^{a,b}, F. Fabozzi^{a,c}, F. Fienga^{a,b}, A.O.M. Iorio^{a,b}, G. Lanza^a, L. Lista^a, S. Meola^{a,d,16}, P. Paolucci^{a,16}, C. Sciacca^{a,b}, F. Thyssen^a

INFN Sezione di Padova^a, Università di Padova^b, Padova, Italy, Università di Trento^c, Trento, Italy

P. Azzi^{a,16}, N. Bacchetta^a, L. Benato^{a,b}, D. Bisello^{a,b}, A. Boletti^{a,b}, R. Carlin^{a,b}, A. Carvalho Antunes De Oliveira^{a,b}, P. Checchia^a, M. Dall'Osso^{a,b}, P. De Castro Manzano^a, T. Dorigo^a, U. Dosselli^a, F. Gasparini^{a,b}, U. Gasparini^{a,b}, S. Lacaprara^a, M. Margoni^{a,b}, A.T. Meneguzzo^{a,b}, J. Pazzini^{a,b}, N. Pozzobon^{a,b}, P. Ronchese^{a,b}, R. Rossin^{a,b}, F. Simonetto^{a,b}, E. Torassa^a, M. Zanetti^{a,b}, P. Zotto^{a,b}, G. Zumerle^{a,b}

INFN Sezione di Pavia^a, Università di Pavia^b, Pavia, Italy

A. Braghieri^a, F. Fallavollita^{a,b}, A. Magnani^{a,b}, P. Montagna^{a,b}, S.P. Ratti^{a,b}, V. Re^a, M. Ressegotti, C. Riccardi^{a,b}, P. Salvini^a, I. Vai^{a,b}, P. Vitulo^{a,b}

INFN Sezione di Perugia^a, Università di Perugia^b, Perugia, Italy

L. Alunni Solestizi^{a,b}, G.M. Bilei^a, D. Ciangottini^{a,b}, L. Fanò^{a,b}, P. Lariccia^{a,b}, R. Leonardi^{a,b}, G. Mantovani^{a,b}, V. Mariani^{a,b}, M. Menichelli^a, A. Saha^a, A. Santocchia^{a,b}

INFN Sezione di Pisa^a, Università di Pisa^b, Scuola Normale Superiore di Pisa^c, Pisa, Italy

K. Androsov^{a,30}, P. Azzurri^{a,16}, G. Bagliesi^a, J. Bernardini^a, T. Boccali^a, R. Castaldi^a, M.A. Ciocci^{a,30}, R. Dell'Orso^a, G. Fedi, A. Giassi^a, M.T. Grippo^{a,30}, F. Ligabue^{a,c}, T. Lomtadze^a, L. Martini^{a,b}, A. Messineo^{a,b}, F. Palla^a, A. Rizzi^{a,b}, A. Savoy-Navarro^{a,31}, P. Spagnolo^a, R. Tenchini^a, G. Tonelli^{a,b}, A. Venturi^a, P.G. Verdini^a

INFN Sezione di Roma[a], Università di Roma[b], Roma, Italy

L. Barone[a,b], F. Cavallari[a], M. Cipriani[a,b], D. Del Re[a,b,16], M. Diemoz[a], S. Gelli[a,b], E. Longo[a,b], F. Margaroli[a,b], B. Marzocchi[a,b], P. Meridiani[a], G. Organtini[a,b], R. Paramatti[a,b], F. Preiato[a,b], S. Rahatlou[a,b], C. Rovelli[a], F. Santanastasio[a,b]

INFN Sezione di Torino[a], Università di Torino[b], Torino, Italy, Università del Piemonte Orientale[c], Novara, Italy

N. Amapane[a,b], R. Arcidiacono[a,c,16], S. Argiro[a,b], M. Arneodo[a,c], N. Bartosik[a], R. Bellan[a,b], C. Biino[a], N. Cartiglia[a], F. Cenna[a,b], M. Costa[a,b], R. Covarelli[a,b], A. Degano[a,b], N. Demaria[a], L. Finco[a,b], B. Kiani[a,b], C. Mariotti[a], S. Maselli[a], E. Migliore[a,b], V. Monaco[a,b], E. Monteil[a,b], M. Monteno[a], M.M. Obertino[a,b], L. Pacher[a,b], N. Pastrone[a], M. Pelliccioni[a], G.L. Pinna Angioni[a,b], F. Ravera[a,b], A. Romero[a,b], M. Ruspa[a,c], R. Sacchi[a,b], K. Shchelina[a,b], V. Sola[a], A. Solano[a,b], A. Staiano[a], P. Traczyk[a,b]

INFN Sezione di Trieste[a], Università di Trieste[b], Trieste, Italy

S. Belforte[a], M. Casarsa[a], F. Cossutti[a], G. Della Ricca[a,b], A. Zanetti[a]

Kyungpook National University, Daegu, Korea

D.H. Kim, G.N. Kim, M.S. Kim, S. Lee, S.W. Lee, Y.D. Oh, S. Sekmen, D.C. Son, Y.C. Yang

Chonbuk National University, Jeonju, Korea

A. Lee

Chonnam National University, Institute for Universe and Elementary Particles, Kwangju, Korea

H. Kim

Hanyang University, Seoul, Korea

J.A. Brochero Cifuentes, T.J. Kim

Korea University, Seoul, Korea

S. Cho, S. Choi, Y. Go, D. Gyun, S. Ha, B. Hong, Y. Jo, Y. Kim, K. Lee, K.S. Lee, S. Lee, J. Lim, S.K. Park, Y. Roh

Seoul National University, Seoul, Korea

J. Almond, J. Kim, H. Lee, S.B. Oh, B.C. Radburn-Smith, S.h. Seo, U.K. Yang, H.D. Yoo, G.B. Yu

University of Seoul, Seoul, Korea

M. Choi, H. Kim, J.H. Kim, J.S.H. Lee, I.C. Park, G. Ryu, M.S. Ryu

Sungkyunkwan University, Suwon, Korea

Y. Choi, J. Goh, C. Hwang, J. Lee, I. Yu

Vilnius University, Vilnius, Lithuania

V. Dudenas, A. Juodagalvis, J. Vaitkus

National Centre for Particle Physics, Universiti Malaya, Kuala Lumpur, Malaysia

I. Ahmed, Z.A. Ibrahim, M.A.B. Md Ali[32], F. Mohamad Idris[33], W.A.T. Wan Abdullah, M.N. Yusli, Z. Zolkapli

Centro de Investigacion y de Estudios Avanzados del IPN, Mexico City, Mexico

H. Castilla-Valdez, E. De La Cruz-Burelo, I. Heredia-De La Cruz[34], A. Hernandez-Almada, R. Lopez-Fernandez, R. Magaña Villalba, J. Mejia Guisao, A. Sanchez-Hernandez

Universidad Iberoamericana, Mexico City, Mexico

S. Carrillo Moreno, C. Oropeza Barrera, F. Vazquez Valencia

Benemerita Universidad Autonoma de Puebla, Puebla, Mexico

S. Carpinteyro, I. Pedraza, H.A. Salazar Ibarguen, C. Uribe Estrada

Universidad Autónoma de San Luis Potosí, San Luis Potosí, Mexico

A. Morelos Pineda

University of Auckland, Auckland, New Zealand

D. Krofcheck

University of Canterbury, Christchurch, New Zealand

P.H. Butler

National Centre for Physics, Quaid-I-Azam University, Islamabad, Pakistan

A. Ahmad, M. Ahmad, Q. Hassan, H.R. Hoorani, W.A. Khan, A. Saddique, M.A. Shah, M. Shoaib, M. Waqas

National Centre for Nuclear Research, Swierk, Poland

H. Bialkowska, M. Bluj, B. Boimska, T. Frueboes, M. Górski, M. Kazana, K. Nawrocki, K. Romanowska-Rybinska, M. Szleper, P. Zalewski

Institute of Experimental Physics, Faculty of Physics, University of Warsaw, Warsaw, Poland

K. Bunkowski, A. Byszuk[35], K. Doroba, A. Kalinowski, M. Konecki, J. Krolikowski, M. Misiura, M. Olszewski, M. Walczak

Laboratório de Instrumentação e Física Experimental de Partículas, Lisboa, Portugal

P. Bargassa, C. Beirão Da Cruz E Silva, B. Calpas, A. Di Francesco, P. Faccioli, M. Gallinaro, J. Hollar, N. Leonardo, L. Lloret Iglesias, M.V. Nemallapudi, J. Seixas, O. Toldaiev, D. Vadruccio, J. Varela

Joint Institute for Nuclear Research, Dubna, Russia

S. Afanasiev, P. Bunin, M. Gavrilenko, I. Golutvin, I. Gorbunov, A. Kamenev, V. Karjavin, A. Lanev, A. Malakhov, V. Matveev[36,37], V. Palichik, V. Perelygin, S. Shmatov, S. Shulha, N. Skatchkov, V. Smirnov, N. Voytishin, A. Zarubin

Petersburg Nuclear Physics Institute, Gatchina (St. Petersburg), Russia

L. Chtchipounov, V. Golovtsov, Y. Ivanov, V. Kim[38], E. Kuznetsova[39], V. Murzin, V. Oreshkin, V. Sulimov, A. Vorobyev

Institute for Nuclear Research, Moscow, Russia

Yu. Andreev, A. Dermenev, S. Gninenko, N. Golubev, A. Karneyeu, M. Kirsanov, N. Krasnikov, A. Pashenkov, D. Tlisov, A. Toropin

Institute for Theoretical and Experimental Physics, Moscow, Russia

V. Epshteyn, V. Gavrilov, N. Lychkovskaya, V. Popov, I. Pozdnyakov, G. Safronov, A. Spiridonov, M. Toms, E. Vlasov, A. Zhokin

Moscow Institute of Physics and Technology, Moscow, Russia

T. Aushev, A. Bylinkin[37]

National Research Nuclear University 'Moscow Engineering Physics Institute' (MEPhI), Moscow, Russia

M. Danilov[40], E. Popova, V. Rusinov

P.N. Lebedev Physical Institute, Moscow, Russia

V. Andreev, M. Azarkin[37], I. Dremin[37], M. Kirakosyan, A. Leonidov[37], A. Terkulov

Skobeltsyn Institute of Nuclear Physics, Lomonosov Moscow State University, Moscow, Russia

A. Baskakov, A. Belyaev, E. Boos, V. Bunichev, M. Dubinin[41], L. Dudko, A. Ershov, A. Gribushin, V. Klyukhin, O. Kodolova, I. Lokhtin, I. Miagkov, S. Obraztsov, V. Savrin, A. Snigirev

Novosibirsk State University (NSU), Novosibirsk, Russia

V. Blinov[42], Y.Skovpen[42], D. Shtol[42]

State Research Center of Russian Federation, Institute for High Energy Physics, Protvino, Russia

I. Azhgirey, I. Bayshev, S. Bitioukov, D. Elumakhov, V. Kachanov, A. Kalinin, D. Konstantinov, V. Krychkine, V. Petrov, R. Ryutin, A. Sobol, S. Troshin, N. Tyurin, A. Uzunian, A. Volkov

University of Belgrade, Faculty of Physics and Vinca Institute of Nuclear Sciences, Belgrade, Serbia

P. Adzic[43], P. Cirkovic, D. Devetak, M. Dordevic, J. Milosevic, V. Rekovic

Centro de Investigaciones Energéticas Medioambientales y Tecnológicas (CIEMAT), Madrid, Spain

J. Alcaraz Maestre, M. Barrio Luna, E. Calvo, M. Cerrada, M. Chamizo Llatas, N. Colino, B. De La Cruz, A. Delgado Peris, A. Escalante Del Valle, C. Fernandez Bedoya, J.P. Fernández Ramos, J. Flix, M.C. Fouz, P. Garcia-Abia, O. Gonzalez Lopez, S. Goy Lopez, J.M. Hernandez, M.I. Josa, E. Navarro De Martino, A. Pérez-Calero Yzquierdo, J. Puerta Pelayo, A. Quintario Olmeda, I. Redondo, L. Romero, M.S. Soares

Universidad Autónoma de Madrid, Madrid, Spain

J.F. de Trocóniz, M. Missiroli, D. Moran

Universidad de Oviedo, Oviedo, Spain

J. Cuevas, C. Erice, J. Fernandez Menendez, I. Gonzalez Caballero, J.R. González Fernández, E. Palencia Cortezon, S. Sanchez Cruz, I. Suárez Andrés, P. Vischia, J.M. Vizan Garcia

Instituto de Física de Cantabria (IFCA), CSIC-Universidad de Cantabria, Santander, Spain

I.J. Cabrillo, A. Calderon, E. Curras, M. Fernandez, J. Garcia-Ferrero, G. Gomez, A. Lopez Virto, J. Marco, C. Martinez Rivero, F. Matorras, J. Piedra Gomez, T. Rodrigo, A. Ruiz-Jimeno, L. Scodellaro, N. Trevisani, I. Vila, R. Vilar Cortabitarte

CERN, European Organization for Nuclear Research, Geneva, Switzerland

D. Abbaneo, E. Auffray, G. Auzinger, P. Baillon, A.H. Ball, D. Barney, P. Bloch, A. Bocci, C. Botta, T. Camporesi, R. Castello, M. Cepeda, G. Cerminara, Y. Chen, A. Cimmino, D. d'Enterria, A. Dabrowski, V. Daponte, A. David, M. De Gruttola, A. De Roeck, E. Di Marco[44], M. Dobson, B. Dorney, T. du Pree, D. Duggan, M. Dünser, N. Dupont, A. Elliott-Peisert, P. Everaerts, S. Fartoukh, G. Franzoni, J. Fulcher, W. Funk, D. Gigi, K. Gill, M. Girone, F. Glege, D. Gulhan, S. Gundacker, M. Guthoff, P. Harris, J. Hegeman, V. Innocente, P. Janot, J. Kieseler, H. Kirschenmann, V. Knünz, A. Kornmayer[16], M.J. Kortelainen, K. Kousouris, M. Krammer[1], C. Lange, P. Lecoq, C. Lourenço, M.T. Lucchini, L. Malgeri, M. Mannelli, A. Martelli, F. Meijers, J.A. Merlin, S. Mersi, E. Meschi, P. Milenovic[45], F. Moortgat, S. Morovic, M. Mulders, H. Neugebauer, S. Orfanelli, L. Orsini, L. Pape, E. Perez, M. Peruzzi, A. Petrilli, G. Petrucciani, A. Pfeiffer, M. Pierini, A. Racz, T. Reis, G. Rolandi[46], M. Rovere, H. Sakulin, J.B. Sauvan, C. Schäfer, C. Schwick, M. Seidel, A. Sharma, P. Silva, P. Sphicas[47], J. Steggemann, M. Stoye, Y. Takahashi, M. Tosi, D. Treille, A. Triossi, A. Tsirou, V. Veckalns[48], G.I. Veres[21], M. Verweij, N. Wardle, H.K. Wöhri, A. Zagozdzinska[35], W.D. Zeuner

Paul Scherrer Institut, Villigen, Switzerland

W. Bertl, K. Deiters, W. Erdmann, R. Horisberger, Q. Ingram, H.C. Kaestli, D. Kotlinski, U. Langenegger, T. Rohe, S.A. Wiederkehr

Institute for Particle Physics, ETH Zurich, Zurich, Switzerland

F. Bachmair, L. Bäni, L. Bianchini, B. Casal, G. Dissertori, M. Dittmar, M. Donegà, C. Grab, C. Heidegger, D. Hits, J. Hoss, G. Kasieczka, W. Lustermann, B. Mangano, M. Marionneau, P. Martinez Ruiz del Arbol, M. Masciovecchio, M.T. Meinhard, D. Meister, F. Micheli, P. Musella, F. Nessi-Tedaldi, F. Pandolfi, J. Pata, F. Pauss, G. Perrin, L. Perrozzi, M. Quittnat, M. Rossini, M. Schönenberger, A. Starodumov[49], V.R. Tavolaro, K. Theofilatos, R. Wallny

Universität Zürich, Zurich, Switzerland

T.K. Aarrestad, C. Amsler[50], L. Caminada, M.F. Canelli, A. De Cosa, S. Donato, C. Galloni, A. Hinzmann, T. Hreus, B. Kilminster, J. Ngadiuba, D. Pinna, G. Rauco, P. Robmann, D. Salerno, C. Seitz, Y. Yang, A. Zucchetta

National Central University, Chung-Li, Taiwan

V. Candelise, C.W. Chen, T.H. Doan, Sh. Jain, R. Khurana, M. Konyushikhin, C.M. Kuo, W. Lin, Y.J. Lu, A. Pozdnyakov, F.Y. Tsai, S.S. Yu

National Taiwan University (NTU), Taipei, Taiwan

Arun Kumar, P. Chang, Y.H. Chang, Y. Chao, K.F. Chen, P.H. Chen, F. Fiori, W.-S. Hou, Y. Hsiung, Y.F. Liu, R.-S. Lu, M. Miñano Moya, E. Paganis, A. Psallidas, J.f. Tsai

Chulalongkorn University, Faculty of Science, Department of Physics, Bangkok, Thailand

B. Asavapibhop, G. Singh, N. Srimanobhas, N. Suwonjandee

Cukurova University - Physics Department, Science and Art Faculty

A. Adiguzel, M.N. Bakirci[51], S. Cerci[52], S. Damarseckin, Z.S. Demiroglu, C. Dozen, I. Dumanoglu, S. Girgis, G. Gokbulut, Y. Guler, I. Hos[53], E.E. Kangal[54], O. Kara, A. Kayis Topaksu, U. Kiminsu, M. Oglakci, G. Onengut[55], K. Ozdemir[56], B. Tali[52], S. Turkcapar, I.S. Zorbakir, C. Zorbilmez

Middle East Technical University, Physics Department, Ankara, Turkey

B. Bilin, S. Bilmis, B. Isildak[57], G. Karapinar[58], M. Yalvac, M. Zeyrek

Bogazici University, Istanbul, Turkey

E. Gülmez, M. Kaya[59], O. Kaya[60], E.A. Yetkin[61], T. Yetkin[62]

Istanbul Technical University, Istanbul, Turkey

A. Cakir, K. Cankocak, S. Sen[63]

Institute for Scintillation Materials of National Academy of Science of Ukraine, Kharkov, Ukraine

B. Grynyov

National Scientific Center, Kharkov Institute of Physics and Technology, Kharkov, Ukraine

L. Levchuk, P. Sorokin

University of Bristol, Bristol, United Kingdom

R. Aggleton, F. Ball, L. Beck, J.J. Brooke, D. Burns, E. Clement, D. Cussans, H. Flacher, J. Goldstein, M. Grimes, G.P. Heath, H.F. Heath, J. Jacob, L. Kreczko, C. Lucas, D.M. Newbold[64], S. Paramesvaran, A. Poll, T. Sakuma, S. Seif El Nasr-storey, D. Smith, V.J. Smith

Rutherford Appleton Laboratory, Didcot, United Kingdom

K.W. Bell, A. Belyaev[65], C. Brew, R.M. Brown, L. Calligaris, D. Cieri, D.J.A. Cockerill, J.A. Coughlan, K. Harder, S. Harper, E. Olaiya, D. Petyt, C.H. Shepherd-Themistocleous, A. Thea, I.R. Tomalin, T. Williams

Imperial College, London, United Kingdom

M. Baber, R. Bainbridge, O. Buchmuller, A. Bundock, S. Casasso, M. Citron, D. Colling, L. Corpe, P. Dauncey, G. Davies, A. De Wit, M. Della Negra, R. Di Maria, P. Dunne, A. Elwood, D. Futyan, Y. Haddad, G. Hall, G. Iles, T. James, R. Lane, C. Laner, L. Lyons, A.-M. Magnan, S. Malik, L. Mastrolorenzo, J. Nash, A. Nikitenko[49], J. Pela, B. Penning, M. Pesaresi, D.M. Raymond, A. Richards, A. Rose, E. Scott, C. Seez, S. Summers, A. Tapper, K. Uchida, M. Vazquez Acosta[66], T. Virdee[16], J. Wright, S.C. Zenz

Brunel University, Uxbridge, United Kingdom

J.E. Cole, P.R. Hobson, A. Khan, P. Kyberd, I.D. Reid, P. Symonds, L. Teodorescu, M. Turner

Baylor University, Waco, U.S.A.

A. Borzou, K. Call, J. Dittmann, K. Hatakeyama, H. Liu, N. Pastika

Catholic University of America

R. Bartek, A. Dominguez

The University of Alabama, Tuscaloosa, U.S.A.

A. Buccilli, S.I. Cooper, C. Henderson, P. Rumerio, C. West

Boston University, Boston, U.S.A.

D. Arcaro, A. Avetisyan, T. Bose, D. Gastler, D. Rankin, C. Richardson, J. Rohlf, L. Sulak, D. Zou

Brown University, Providence, U.S.A.

G. Benelli, D. Cutts, A. Garabedian, J. Hakala, U. Heintz, J.M. Hogan, O. Jesus, K.H.M. Kwok, E. Laird, G. Landsberg, Z. Mao, M. Narain, S. Piperov, S. Sagir, E. Spencer, R. Syarif

University of California, Davis, Davis, U.S.A.

R. Breedon, D. Burns, M. Calderon De La Barca Sanchez, S. Chauhan, M. Chertok, J. Conway, R. Conway, P.T. Cox, R. Erbacher, C. Flores, G. Funk, M. Gardner, W. Ko, R. Lander, C. Mclean, M. Mulhearn, D. Pellett, J. Pilot, S. Shalhout, M. Shi, J. Smith, M. Squires, D. Stolp, K. Tos, M. Tripathi

University of California, Los Angeles, U.S.A.

M. Bachtis, C. Bravo, R. Cousins, A. Dasgupta, A. Florent, J. Hauser, M. Ignatenko, N. Mccoll, D. Saltzberg, C. Schnaible, V. Valuev, M. Weber

University of California, Riverside, Riverside, U.S.A.

E. Bouvier, K. Burt, R. Clare, J. Ellison, J.W. Gary, S.M.A. Ghiasi Shirazi, G. Hanson, J. Heilman, P. Jandir, E. Kennedy, F. Lacroix, O.R. Long, M. Olmedo Negrete, M.I. Paneva, A. Shrinivas, W. Si, H. Wei, S. Wimpenny, B. R. Yates

University of California, San Diego, La Jolla, U.S.A.

J.G. Branson, G.B. Cerati, S. Cittolin, M. Derdzinski, R. Gerosa, A. Holzner, D. Klein, V. Krutelyov, J. Letts, I. Macneill, D. Olivito, S. Padhi, M. Pieri, M. Sani, V. Sharma, S. Simon, M. Tadel, A. Vartak, S. Wasserbaech[67], C. Welke, J. Wood, F. Würthwein, A. Yagil, G. Zevi Della Porta

University of California, Santa Barbara - Department of Physics, Santa Barbara, U.S.A.

N. Amin, R. Bhandari, J. Bradmiller-Feld, C. Campagnari, A. Dishaw, V. Dutta, M. Franco Sevilla, C. George, F. Golf, L. Gouskos, J. Gran, R. Heller, J. Incandela, S.D. Mullin, A. Ovcharova, H. Qu, J. Richman, D. Stuart, I. Suarez, J. Yoo

California Institute of Technology, Pasadena, U.S.A.

D. Anderson, J. Bendavid, A. Bornheim, J. Bunn, J. Duarte, J.M. Lawhorn, A. Mott, H.B. Newman, C. Pena, M. Spiropulu, J.R. Vlimant, S. Xie, R.Y. Zhu

Carnegie Mellon University, Pittsburgh, U.S.A.

M.B. Andrews, T. Ferguson, M. Paulini, J. Russ, M. Sun, H. Vogel, I. Vorobiev, M. Weinberg

University of Colorado Boulder, Boulder, U.S.A.

J.P. Cumalat, W.T. Ford, F. Jensen, A. Johnson, M. Krohn, S. Leontsinis, T. Mulholland, K. Stenson, S.R. Wagner

Cornell University, Ithaca, U.S.A.

J. Alexander, J. Chaves, J. Chu, S. Dittmer, K. Mcdermott, N. Mirman, J.R. Patterson, A. Rinkevicius, A. Ryd, L. Skinnari, L. Soffi, S.M. Tan, Z. Tao, J. Thom, J. Tucker, P. Wittich, M. Zientek

Fairfield University, Fairfield, U.S.A.

D. Winn

Fermi National Accelerator Laboratory, Batavia, U.S.A.

S. Abdullin, M. Albrow, G. Apollinari, A. Apresyan, S. Banerjee, L.A.T. Bauerdick, A. Beretvas, J. Berryhill, P.C. Bhat, G. Bolla, K. Burkett, J.N. Butler, H.W.K. Cheung, F. Chlebana, S. Cihangir[†], M. Cremonesi, V.D. Elvira, I. Fisk, J. Freeman, E. Gottschalk, L. Gray, D. Green, S. Grünendahl, O. Gutsche, D. Hare, R.M. Harris, S. Hasegawa, J. Hirschauer, Z. Hu, B. Jayatilaka, S. Jindariani, M. Johnson, U. Joshi, B. Klima, B. Kreis, S. Lammel, J. Linacre, D. Lincoln, R. Lipton, M. Liu, T. Liu, R. Lopes De Sá, J. Lykken, K. Maeshima, N. Magini, J.M. Marraffino, S. Maruyama, D. Mason, P. McBride, P. Merkel, S. Mrenna, S. Nahn, V. O'Dell, K. Pedro, O. Prokofyev, G. Rakness, L. Ristori, E. Sexton-Kennedy, A. Soha, W.J. Spalding, L. Spiegel, S. Stoynev, J. Strait, N. Strobbe, L. Taylor, S. Tkaczyk, N.V. Tran, L. Uplegger, E.W. Vaandering, C. Vernieri, M. Verzocchi, R. Vidal, M. Wang, H.A. Weber, A. Whitbeck, Y. Wu

University of Florida, Gainesville, U.S.A.

D. Acosta, P. Avery, P. Bortignon, D. Bourilkov, A. Brinkerhoff, A. Carnes, M. Carver, D. Curry, S. Das, R.D. Field, I.K. Furic, J. Konigsberg, A. Korytov, J.F. Low, P. Ma, K. Matchev, H. Mei, G. Mitselmakher, D. Rank, L. Shchutska, D. Sperka, L. Thomas, J. Wang, S. Wang, J. Yelton

Florida International University, Miami, U.S.A.

S. Linn, P. Markowitz, G. Martinez, J.L. Rodriguez

Florida State University, Tallahassee, U.S.A.

A. Ackert, T. Adams, A. Askew, S. Bein, S. Hagopian, V. Hagopian, K.F. Johnson, T. Kolberg, T. Perry, H. Prosper, A. Santra, R. Yohay

Florida Institute of Technology, Melbourne, U.S.A.

M.M. Baarmand, V. Bhopatkar, S. Colafranceschi, M. Hohlmann, D. Noonan, T. Roy, F. Yumiceva

University of Illinois at Chicago (UIC), Chicago, U.S.A.

M.R. Adams, L. Apanasevich, D. Berry, R.R. Betts, R. Cavanaugh, X. Chen, O. Evdokimov, C.E. Gerber, D.A. Hangal, D.J. Hofman, K. Jung, J. Kamin, I.D. Sandoval Gonzalez, H. Trauger, N. Varelas, H. Wang, Z. Wu, M. Zakaria, J. Zhang

The University of Iowa, Iowa City, U.S.A.

B. Bilki[68], W. Clarida, K. Dilsiz, S. Durgut, R.P. Gandrajula, M. Haytmyradov, V. Khristenko, J.-P. Merlo, H. Mermerkaya[69], A. Mestvirishvili, A. Moeller, J. Nachtman, H. Ogul, Y. Onel, F. Ozok[70], A. Penzo, C. Snyder, E. Tiras, J. Wetzel, K. Yi

Johns Hopkins University, Baltimore, U.S.A.

B. Blumenfeld, A. Cocoros, N. Eminizer, D. Fehling, L. Feng, A.V. Gritsan, P. Maksimovic, J. Roskes, U. Sarica, M. Swartz, M. Xiao, C. You

The University of Kansas, Lawrence, U.S.A.

A. Al-bataineh, P. Baringer, A. Bean, S. Boren, J. Bowen, J. Castle, L. Forthomme, S. Khalil, A. Kropivnitskaya, D. Majumder, W. Mcbrayer, M. Murray, S. Sanders, R. Stringer, J.D. Tapia Takaki, Q. Wang

Kansas State University, Manhattan, U.S.A.

A. Ivanov, K. Kaadze, Y. Maravin, A. Mohammadi, L.K. Saini, N. Skhirtladze, S. Toda

Lawrence Livermore National Laboratory, Livermore, U.S.A.

F. Rebassoo, D. Wright

University of Maryland, College Park, U.S.A.

C. Anelli, A. Baden, O. Baron, A. Belloni, B. Calvert, S.C. Eno, C. Ferraioli, J.A. Gomez, N.J. Hadley, S. Jabeen, G.Y. Jeng, R.G. Kellogg, J. Kunkle, A.C. Mignerey, F. Ricci-Tam, Y.H. Shin, A. Skuja, M.B. Tonjes, S.C. Tonwar

Massachusetts Institute of Technology, Cambridge, U.S.A.

D. Abercrombie, B. Allen, A. Apyan, V. Azzolini, R. Barbieri, A. Baty, R. Bi, K. Bierwagen, S. Brandt, W. Busza, I.A. Cali, M. D'Alfonso, Z. Demiragli, G. Gomez Ceballos, M. Goncharov, D. Hsu, Y. Iiyama, G.M. Innocenti, M. Klute, D. Kovalskyi, K. Krajczar, Y.S. Lai, Y.-J. Lee, A. Levin, P.D. Luckey, B. Maier, A.C. Marini, C. Mcginn, C. Mironov, S. Narayanan, X. Niu, C. Paus, C. Roland, G. Roland, J. Salfeld-Nebgen, G.S.F. Stephans, K. Tatar, D. Velicanu, J. Wang, T.W. Wang, B. Wyslouch

University of Minnesota, Minneapolis, U.S.A.

A.C. Benvenuti, R.M. Chatterjee, A. Evans, P. Hansen, S. Kalafut, S.C. Kao, Y. Kubota, Z. Lesko, J. Mans, S. Nourbakhsh, N. Ruckstuhl, R. Rusack, N. Tambe, J. Turkewitz

University of Mississippi, Oxford, U.S.A.

J.G. Acosta, S. Oliveros

University of Nebraska-Lincoln, Lincoln, U.S.A.

E. Avdeeva, K. Bloom, D.R. Claes, C. Fangmeier, R. Gonzalez Suarez, R. Kamalieddin, I. Kravchenko, A. Malta Rodrigues, J. Monroy, J.E. Siado, G.R. Snow, B. Stieger

State University of New York at Buffalo, Buffalo, U.S.A.

M. Alyari, J. Dolen, A. Godshalk, C. Harrington, I. Iashvili, J. Kaisen, D. Nguyen, A. Parker, S. Rappoccio, B. Roozbahani

Northeastern University, Boston, U.S.A.

G. Alverson, E. Barberis, A. Hortiangtham, A. Massironi, D.M. Morse, D. Nash, T. Orimoto, R. Teixeira De Lima, D. Trocino, R.-J. Wang, D. Wood

Northwestern University, Evanston, U.S.A.

S. Bhattacharya, O. Charaf, K.A. Hahn, N. Mucia, N. Odell, B. Pollack, M.H. Schmitt, K. Sung, M. Trovato, M. Velasco

University of Notre Dame, Notre Dame, U.S.A.

N. Dev, M. Hildreth, K. Hurtado Anampa, C. Jessop, D.J. Karmgard, N. Kellams, K. Lannon, N. Marinelli, F. Meng, C. Mueller, Y. Musienko[36], M. Planer, A. Reinsvold, R. Ruchti, N. Rupprecht, G. Smith, S. Taroni, M. Wayne, M. Wolf, A. Woodard

The Ohio State University, Columbus, U.S.A.

J. Alimena, L. Antonelli, B. Bylsma, L.S. Durkin, S. Flowers, B. Francis, A. Hart, C. Hill, W. Ji, B. Liu, W. Luo, D. Puigh, B.L. Winer, H.W. Wulsin

Princeton University, Princeton, U.S.A.

S. Cooperstein, O. Driga, P. Elmer, J. Hardenbrook, P. Hebda, D. Lange, J. Luo, D. Marlow, T. Medvedeva, K. Mei, I. Ojalvo, J. Olsen, C. Palmer, P. Piroué, D. Stickland, A. Svyatkovskiy, C. Tully

University of Puerto Rico, Mayaguez, U.S.A.

S. Malik

Purdue University, West Lafayette, U.S.A.

A. Barker, V.E. Barnes, S. Folgueras, L. Gutay, M.K. Jha, M. Jones, A.W. Jung, A. Khatiwada, D.H. Miller, N. Neumeister, J.F. Schulte, X. Shi, J. Sun, F. Wang, W. Xie

Purdue University Northwest, Hammond, U.S.A.

N. Parashar, J. Stupak

Rice University, Houston, U.S.A.

A. Adair, B. Akgun, Z. Chen, K.M. Ecklund, F.J.M. Geurts, M. Guilbaud, W. Li, B. Michlin, M. Northup, B.P. Padley, J. Roberts, J. Rorie, Z. Tu, J. Zabel

University of Rochester, Rochester, U.S.A.

B. Betchart, A. Bodek, P. de Barbaro, R. Demina, Y.t. Duh, T. Ferbel, M. Galanti, A. Garcia-Bellido, J. Han, O. Hindrichs, A. Khukhunaishvili, K.H. Lo, P. Tan, M. Verzetti

Rutgers, The State University of New Jersey, Piscataway, U.S.A.

A. Agapitos, J.P. Chou, Y. Gershtein, T.A. Gómez Espinosa, E. Halkiadakis, M. Heindl, E. Hughes, S. Kaplan, R. Kunnawalkam Elayavalli, S. Kyriacou, A. Lath, R. Montalvo, K. Nash, M. Osherson, H. Saka, S. Salur, S. Schnetzer, D. Sheffield, S. Somalwar, R. Stone, S. Thomas, P. Thomassen, M. Walker

University of Tennessee, Knoxville, U.S.A.

A.G. Delannoy, M. Foerster, J. Heideman, G. Riley, K. Rose, S. Spanier, K. Thapa

Texas A&M University, College Station, U.S.A.

O. Bouhali[71], A. Celik, M. Dalchenko, M. De Mattia, A. Delgado, S. Dildick, R. Eusebi, J. Gilmore, T. Huang, E. Juska, T. Kamon[72], R. Mueller, Y. Pakhotin, R. Patel, A. Perloff, L. Perniè, D. Rathjens, A. Safonov, A. Tatarinov, K.A. Ulmer

Texas Tech University, Lubbock, U.S.A.

N. Akchurin, J. Damgov, F. De Guio, C. Dragoiu, P.R. Dudero, J. Faulkner, E. Gurpinar, S. Kunori, K. Lamichhane, S.W. Lee, T. Libeiro, T. Peltola, S. Undleeb, I. Volobouev, Z. Wang

Vanderbilt University, Nashville, U.S.A.

S. Greene, A. Gurrola, R. Janjam, W. Johns, C. Maguire, A. Melo, H. Ni, P. Sheldon, S. Tuo, J. Velkovska, Q. Xu

University of Virginia, Charlottesville, U.S.A.

M.W. Arenton, P. Barria, B. Cox, R. Hirosky, A. Ledovskoy, H. Li, C. Neu, T. Sinthuprasith, X. Sun, Y. Wang, E. Wolfe, F. Xia

Wayne State University, Detroit, U.S.A.

C. Clarke, R. Harr, P.E. Karchin, J. Sturdy, S. Zaleski

University of Wisconsin - Madison, Madison, WI, U.S.A.

D.A. Belknap, J. Buchanan, C. Caillol, S. Dasu, L. Dodd, S. Duric, B. Gomber, M. Grothe, M. Herndon, A. Hervé, U. Hussain, P. Klabbers, A. Lanaro, A. Levine, K. Long, R. Loveless, G.A. Pierro, G. Polese, T. Ruggles, A. Savin, N. Smith, W.H. Smith, D. Taylor, N. Woods

†: Deceased
1: Also at Vienna University of Technology, Vienna, Austria
2: Also at State Key Laboratory of Nuclear Physics and Technology, Peking University, Beijing, China
3: Also at Universidade Estadual de Campinas, Campinas, Brazil
4: Also at Universidade Federal de Pelotas, Pelotas, Brazil
5: Also at Université Libre de Bruxelles, Bruxelles, Belgium
6: Also at Universidad de Antioquia, Medellin, Colombia
7: Also at Joint Institute for Nuclear Research, Dubna, Russia
8: Also at Helwan University, Cairo, Egypt
9: Now at Zewail City of Science and Technology, Zewail, Egypt
10: Now at Fayoum University, El-Fayoum, Egypt
11: Also at British University in Egypt, Cairo, Egypt
12: Now at Ain Shams University, Cairo, Egypt
13: Also at Université de Haute Alsace, Mulhouse, France
14: Also at Skobeltsyn Institute of Nuclear Physics, Lomonosov Moscow State University, Moscow, Russia
15: Also at Tbilisi State University, Tbilisi, Georgia
16: Also at CERN, European Organization for Nuclear Research, Geneva, Switzerland
17: Also at RWTH Aachen University, III. Physikalisches Institut A, Aachen, Germany
18: Also at University of Hamburg, Hamburg, Germany
19: Also at Brandenburg University of Technology, Cottbus, Germany
20: Also at Institute of Nuclear Research ATOMKI, Debrecen, Hungary
21: Also at MTA-ELTE Lendület CMS Particle and Nuclear Physics Group, Eötvös Loránd University, Budapest, Hungary
22: Also at Institute of Physics, University of Debrecen, Debrecen, Hungary
23: Also at Indian Institute of Technology Bhubaneswar, Bhubaneswar, India
24: Also at University of Visva-Bharati, Santiniketan, India
25: Also at Institute of Physics, Bhubaneswar, India
26: Also at University of Ruhuna, Matara, Sri Lanka
27: Also at Isfahan University of Technology, Isfahan, Iran
28: Also at Yazd University, Yazd, Iran
29: Also at Plasma Physics Research Center, Science and Research Branch, Islamic Azad University, Tehran, Iran
30: Also at Università degli Studi di Siena, Siena, Italy
31: Also at Purdue University, West Lafayette, U.S.A.
32: Also at International Islamic University of Malaysia, Kuala Lumpur, Malaysia
33: Also at Malaysian Nuclear Agency, MOSTI, Kajang, Malaysia
34: Also at Consejo Nacional de Ciencia y Tecnología, Mexico city, Mexico
35: Also at Warsaw University of Technology, Institute of Electronic Systems, Warsaw, Poland
36: Also at Institute for Nuclear Research, Moscow, Russia

37: Now at National Research Nuclear University 'Moscow Engineering Physics Institute' (MEPhI), Moscow, Russia

38: Also at St. Petersburg State Polytechnical University, St. Petersburg, Russia

39: Also at University of Florida, Gainesville, U.S.A.

40: Also at P.N. Lebedev Physical Institute, Moscow, Russia

41: Also at California Institute of Technology, Pasadena, U.S.A.

42: Also at Budker Institute of Nuclear Physics, Novosibirsk, Russia

43: Also at Faculty of Physics, University of Belgrade, Belgrade, Serbia

44: Also at INFN Sezione di Roma; Università di Roma, Roma, Italy

45: Also at University of Belgrade, Faculty of Physics and Vinca Institute of Nuclear Sciences, Belgrade, Serbia

46: Also at Scuola Normale e Sezione dell'INFN, Pisa, Italy

47: Also at National and Kapodistrian University of Athens, Athens, Greece

48: Also at Riga Technical University, Riga, Latvia

49: Also at Institute for Theoretical and Experimental Physics, Moscow, Russia

50: Also at Albert Einstein Center for Fundamental Physics, Bern, Switzerland

51: Also at Gaziosmanpasa University, Tokat, Turkey

52: Also at Adiyaman University, Adiyaman, Turkey

53: Also at Istanbul Aydin University, Istanbul, Turkey

54: Also at Mersin University, Mersin, Turkey

55: Also at Cag University, Mersin, Turkey

56: Also at Piri Reis University, Istanbul, Turkey

57: Also at Ozyegin University, Istanbul, Turkey

58: Also at Izmir Institute of Technology, Izmir, Turkey

59: Also at Marmara University, Istanbul, Turkey

60: Also at Kafkas University, Kars, Turkey

61: Also at Istanbul Bilgi University, Istanbul, Turkey

62: Also at Yildiz Technical University, Istanbul, Turkey

63: Also at Hacettepe University, Ankara, Turkey

64: Also at Rutherford Appleton Laboratory, Didcot, United Kingdom

65: Also at School of Physics and Astronomy, University of Southampton, Southampton, United Kingdom

66: Also at Instituto de Astrofísica de Canarias, La Laguna, Spain

67: Also at Utah Valley University, Orem, U.S.A.

68: Also at BEYKENT UNIVERSITY, Istanbul, Turkey

69: Also at Erzincan University, Erzincan, Turkey

70: Also at Mimar Sinan University, Istanbul, Istanbul, Turkey

71: Also at Texas A&M University at Qatar, Doha, Qatar

72: Also at Kyungpook National University, Daegu, Korea